(1)

Communications Research Centre

PHASE COHERENCE AND SIGNAL-TO-NOISE RATIO CONSIDERATIONS FOR SAMPLED APERTURE RADAR SYSTEMS

by

J. Litva and H.C. Chan

This work was sponsored by Department of National Defence, Research and Development Branch under Project No. 011LA.

CRC REPORT NO. 1412
OTTAWA, DECEMBER 1987

Government of Canada
Department of Communications

Gouvernement du Canada
Ministère des Communications

Canada

COMMUNICATIONS RESEARCH CENTRE

DEPARTMENT OF COMMUNICATIONS
CANADA

PHASE COHERENCE AND SIGNAL-TO-NOISE RATIO CONSIDERATIONS FOR SAMPLED APERTURE RADAR SYSTEMS

by

J. Litva and H.C. Chan

(Radar and Communications Technology Branch)

CRC REPORT NO. 1412

December 1987
OTTAWA

This work was sponsored by the Department of National Defence, Research and Development Branch under Project No.011LA.

TABLE OF CONTENTS

PHASE COHERENCE AND SIGNAL-TO-NOISE RATIO CONSIDERATIONS FOR SAMPLED APERTURE RADAR SYSTEMS

by
J. Litva and H.C. Chan

ABSTRACT

This report describes the application of Sampled Aperture Radar (SAMPAR) technology to the tracking of low-angle targets at sea. In particular, expressions are developed and presented describing aperture signals for a conventional (SAMPAR) configuration which uses coherent local oscillators. The radar signals are shown to contain an interference term in which is contained all of the information used during Correlation Height Analysis (CHA) processing. A continuous wave (CW) experiment designed to evaluate the CHA algorithm is described. This system employs a beacon source and self-cohering receivers. It is shown that the same interference term is also contained in the self-cohered received signal. Some pre-processing of the interference term is required prior to CHA processing to optimize the results. A discussion is given of the implementation of Doppler processing for various target velocities. Finally a discussion is given of signal-to-noise ratios for typical target geometries and sea-state conditions, in which forward-scatter clutter, back-scatter clutter and system noise are taken into account.

1. INTRODUCTION

Modern radars rely more and more on digital signal processing. As a result of recent advancement in digital signal processing hardware and software, sampled aperture radar (SAMPAR) systems have become feasible. Figure 1 gives a block diagram of a standard SAMPAR system [1]. As depicted, it is a conventional radar system except for the fact that beamforming is carried out digitally. This results in a system having multiple beams in place of a single beam [2, p.307]. Many signal processing techniques designed to enhance radar performance depend on the radar's ability to maintain phase coherence over a reasonable period of time. These include Doppler processing, Moving Target Indicator (MTI) filtering and synthetic aperture imaging, etc. Doppler processing, as is the case for a conventional radar, is shown in Figure 1 as a means of increasing the radar's sensitivity with respect to clutter. This takes advantage of the fact that in frequency-space the returns from a moving target can be displaced with respect to clutter and therefore are amenable to filtering. Also, Doppler processing gives an independent measurement of the target's radial velocity. Since the processing is carried out in the temporal domain, one requires a phase history of the transmitted signal. In this report we will also see instances of spatial processing, where phase coherence is required between spatial samples which are taken simultaneously in time. In fact, digital beamforming is often implemented using spatial Fourier processing.

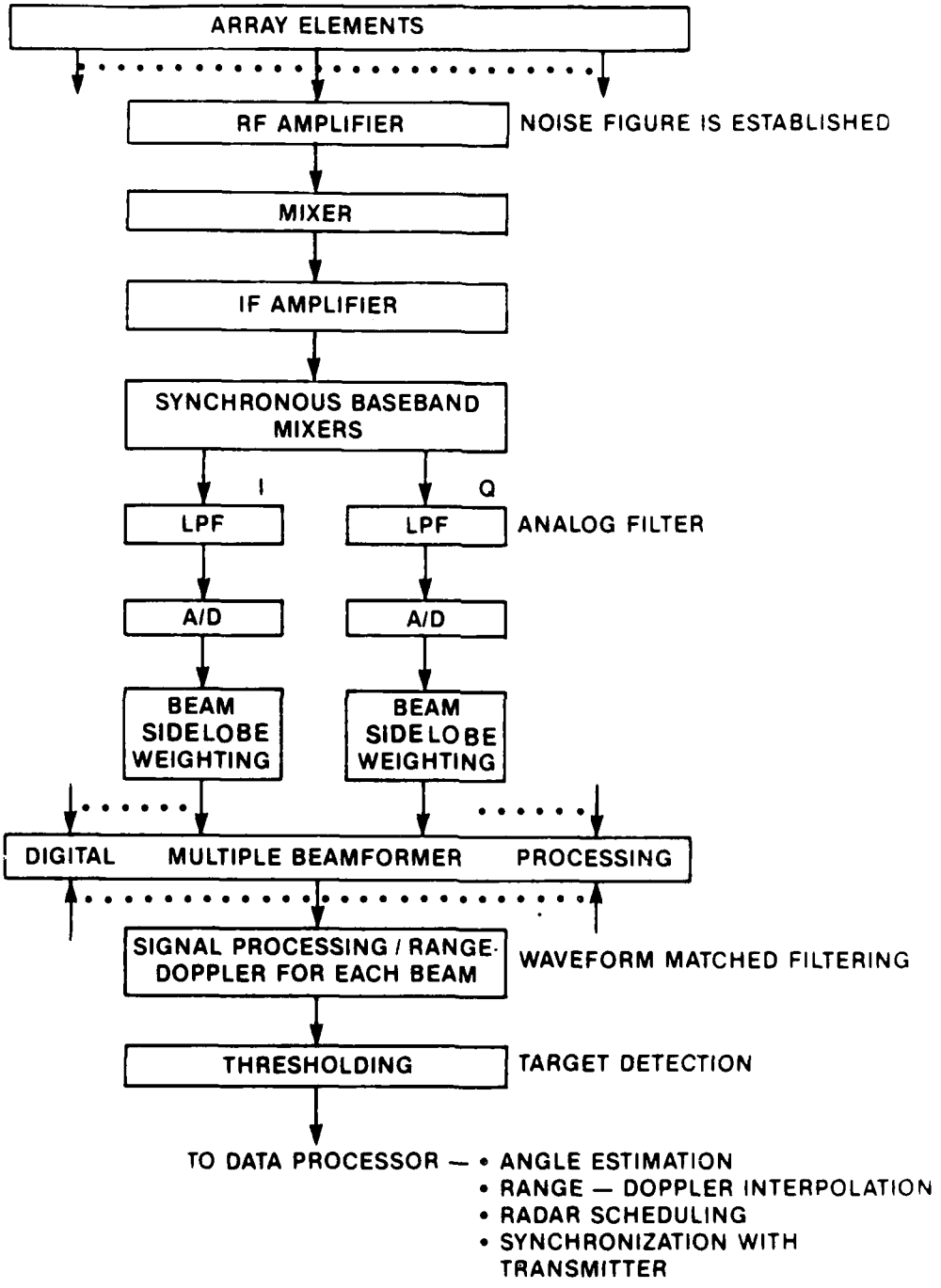

Figure 1 - Block Diagram for Describing Digital Multiple Beamforming (After" Ruvin and Weinburg [1])

2. PHASE COHERENCE AND DIGITAL SIGNAL PROCESSING

In a pulse Doppler radar, phase coherence must be preserved throughout the sampling interval used in the Fourier processing. As is well known, system coherence is usually achieved using a Stalo (Stable local oscillator) and a Coho (coherent local oscillator), as shown in Figure 2 [2]. The MTI radar in Figure 2 is self correcting to the extent that short term errors in f_c and f_ℓ occurring during signal generation are cancelled on reception. For efficient Fourier processing, the stability of both the Stalo and Coho must be sufficiently high that the magnitude of the interpulse frequency drift can be considered to be insignificant. As the stability of these oscillators degrades, coherent integration gain is reduced, i.e. Doppler artifacts are created, thereby increasing the noise floor.

2.1 Baseband Digital Beamforming

The fundamentals of baseband digital beamforming [1] are given in Figure 3. The transmitted signal is

$$f(t)\, e^{j2\pi f_o t} \tag{1}$$

where f(t) describes the amplitude modulation, antenna gain, transmitter power, etc. The transmitter frequency, f_o is equal to $f_\ell + f_c$ using the notation given in Figure 2. The signal received at antenna element k is

$$s_k(t) = f(t-\tau_r)\, e^{j(2\pi f_d t+\phi)}\, e^{j2\pi f_o (t+k\frac{d\cos\alpha}{c})} \tag{2}$$

where τ_r = round-trip target time delay,

f_d = Doppler frequency,

ϕ = arbitrary phase constant, and

$\frac{d\cos\alpha}{c}$ = inter-element time delay.

After synchronous detection, Eqn. (2) becomes

$$s_k(t) = f(t-\tau_r)\, e^{j(2\pi f_d t+\phi)}\, e^{j2\pi k\frac{d\cos\alpha}{\lambda}} \quad . \tag{3}$$

In a SAMPAR system, beamforming is usually implemented using a Fourier transform - i.e. applying Fourier processing to the spatial domain represented by the SAMPAR antenna elements. Rather than being transformed into the frequency domain, as in the case of temporal processing, the

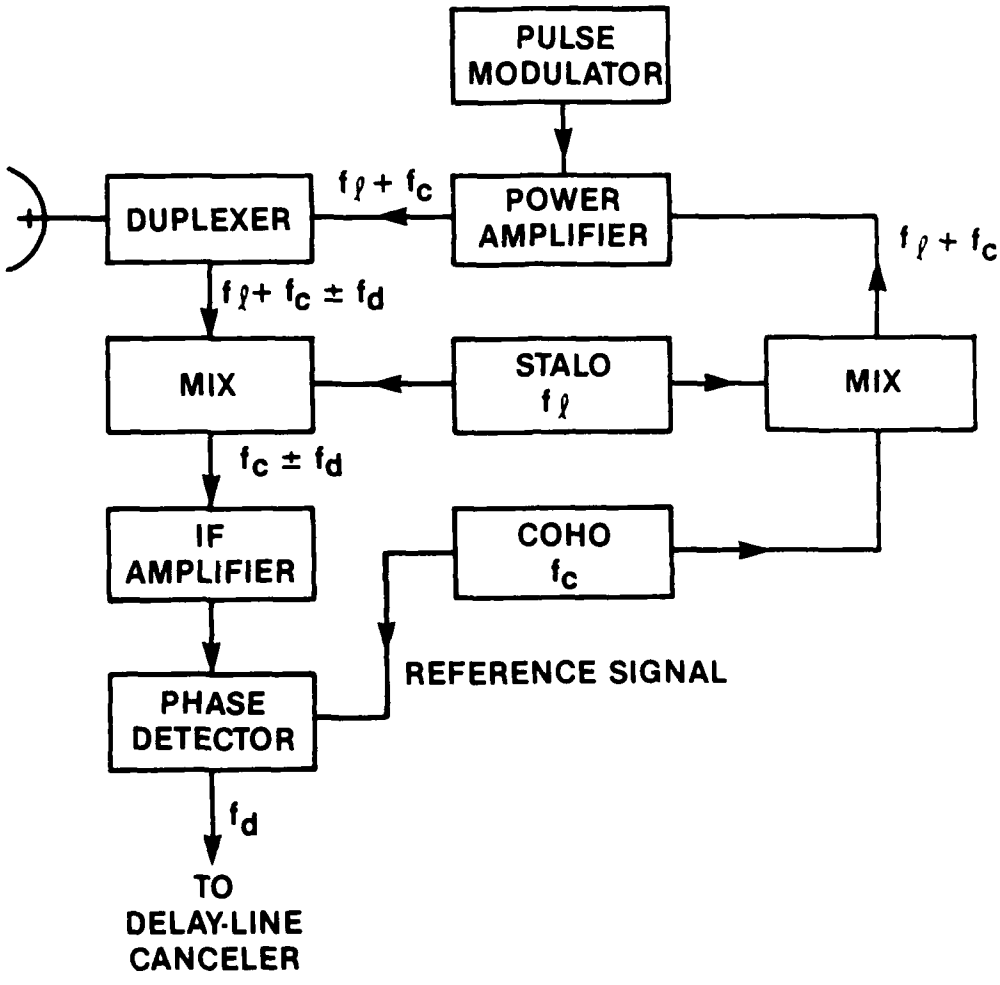

Figure 2 - Block Diagram of a Conventional MTI Radar (After" Skolinik [2])

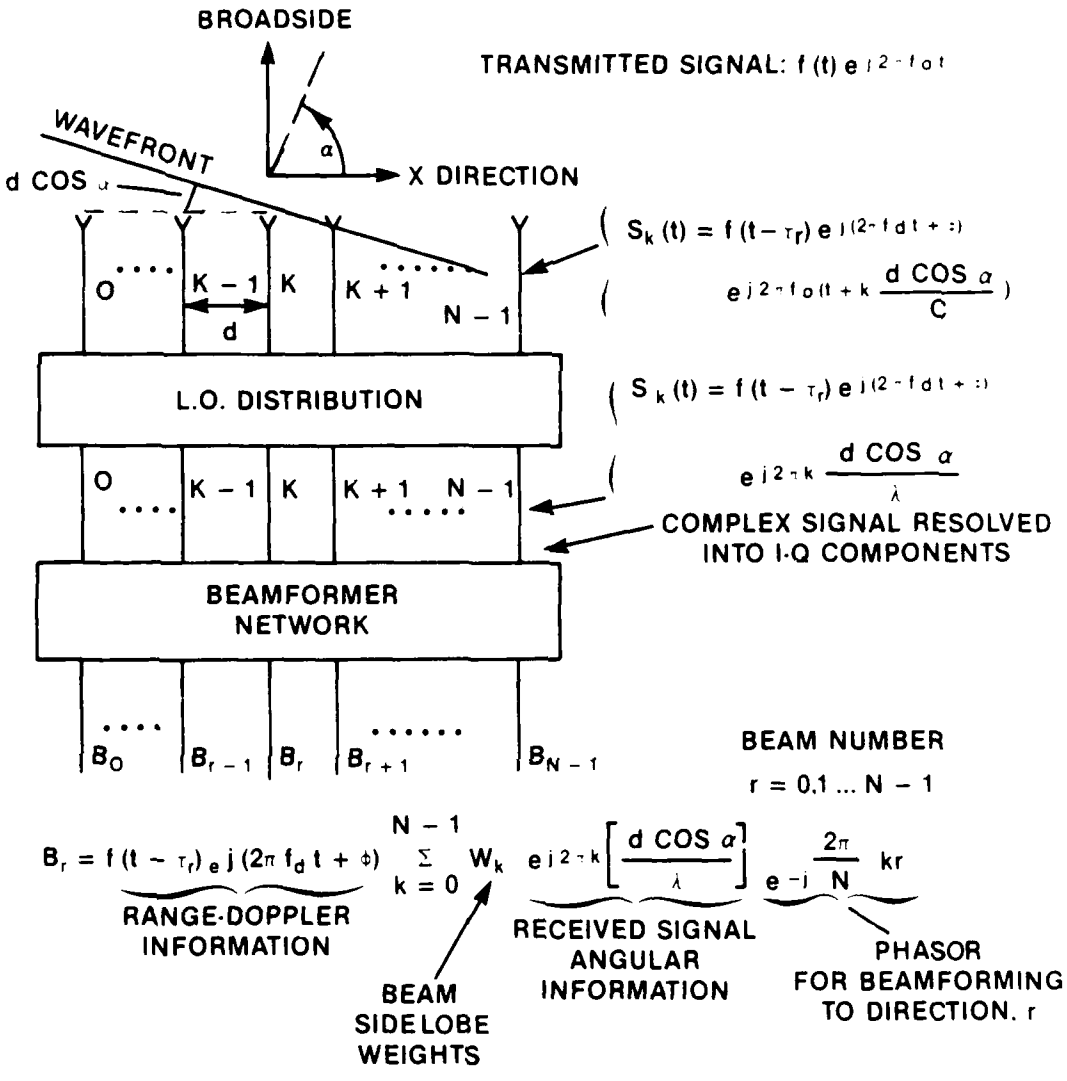

- BEAM, B_r, CONTAINS TARGET AT ANGLE α IF $r \cong \frac{N d \cos \alpha}{\lambda}$
- BEAMFORMING INVOLVES TAKING A DFT OF THE ELEMENT SIGNALS

DFT = Discrete Fourier Transform

Figure 3 - Baseline Beamforming Fundamentals
(After" Ruvin and Weinburg [1])

transform in this case is into beam-space. Fourier processing in digital domain is carried out using the discrete Fourier transform (DFT) or Fast Fourier Transform (FFT). The result of spatial DFT processing is given by

$$B_r = f(t-\tau_r)e^{j(2\pi f_d t+\phi)} \sum_{k=o}^{N-1} W_k\, e^{-j\frac{2\pi}{N}kr}\, e^{j2\pi k[\frac{d\cos\alpha}{\lambda}]}, \qquad (4)$$

range-Doppler information | Phasor for beamforming to direction r | received signal angular information

where B_r gives the response of beam r and the W_k are weights for reducing the sidelobe levels. In addition to system noise, the response B_r will consist of target and clutter signals whose angle-of-arrival α satisfies

$$r \simeq \frac{N d\cos\alpha}{\lambda} .$$

The term $[d\cos\alpha/\lambda]$ represents the analogue angular frequency. For a broadside wavefront, $\alpha = 90°$, the angular frequency is zero and the phase variation from element to element is zero. For $\alpha = 0$ the angular frequency is d/λ and the phase variation from element to element is $(2\pi)d/\lambda$. At some intermediate angle, A, the phase difference between element 0 and k is $(2\pi)[\frac{d}{\lambda}\cos A](k)$. This can be made to look similar to the expression for phase in the conventional sense of frequency, i.e., $(2\pi)[f](t)$, if the analogue of time for spatial filtering is k, and the analogue of f is $\frac{d}{\lambda}\cos\alpha$.

It should be noted that an underlying assumption used in deriving Eqn. (4) is that the radar bandwidth is small compared to radar frequency f_o. If this is not true, as is the case for sonar, temporal Fourier processing must be carried out prior to beamforming. Basically, by doing the temporal processing first, the sonar's bandwidth is divided into smaller segments, and beamforming is applied to each segment. By this method a wideband system can be reduced to a number of narrowband systems [3]. Alternatively, beamforming can be implemented using physical time delays. This alternative is a common form of broadband beamforming.

For FFT processing the number of unique spatial components is equal to the number of sensors or antenna elements. Since the number of elements is limited, a plot of B_r versus α produces an irregular beam

shape which is only a rough approximation to the normal smooth beam shape. In order to obtain smooth beams, with the attending benefit of obtaining finer resolution in direction-finding, smoothing by interpolation must be carried out. Smoothing can be achieved in two ways: (a) using a post-beamforming interpolation algorithm, or (b) by increasing the order of the DFT in Figure 3 and padding the input sequence to the DFT with zeros.

2.2 CHA Processing

The Correlation Height Analysis (CHA) algorithm [4] is a super resolution technique specifically designed to process radar data containing correlated multipath signals. The objective of CHA processing is to resolve a target from its image when their separation is only a small fraction of a beamwidth. Like many other superresolution algorithms, CHA is implemented prior to beamforming. Conventional beamforming is not a requirement of this form of processing. This class of processing uses the complex samples appearing directly after the LPFs and A/Ds in Figure 1. Some signal conditioning is required before CHA processing because of the high SNR requirements of the CHA track selection processor.

The CHA algorithm is similar to the maximum likelihood method [5]. In the maximum likelihood method, one is given a set of observations which may be contaminated by noise or interference. The requirement is to determine what scenario is most likely to have produced the given set of observations. The contamination is represented by the receiver noise. For low-angle tracking problems, it is assumed that there are two plane waves impinging on the antenna aperture. Additional conditions may be imposed on the problem formulation by assuming that there are more than two plane wave fronts if the situation warrants. It is required that the target height (or, equivalently, the target elevation angle) be estimated from the observed composite signal. The CHA algorithm goes one step further by employing a physical model which provides the proper relationship between the two plane waves, i.e., it adds additional a priori information not usually utilized in conventional maximum likelihood methods.

In the past, radar engineers have attempted to solve the low-angle tracking problem by removing the indirect wave component from the composite signal. The CHA algorithm, on the other hand, makes use of the information contained in both the direct and the indirect waves through the use of models of the observed interference pattern. The evolution of the CHA algorithm can be traced back to this attempt to model the interference pattern as a function of target height.

The most effective antenna configuration for CHA processing consists of a vertical sampled aperture. When dealing with the simplest form of the multipath problem, the signal at element k of the array (Figure 3) can be shown to consist of the sum of two signals, a direct signal and an indirect signal and can be written as:

$$s_k^m(t) = f(t-\tau_r)e^{j(2\pi f_d t + \phi_1)}\, e^{j2\pi k \frac{d}{\lambda}\cos\alpha_1} + \rho\, Df(t-\tau_r)e^{j(2\pi f_d t + \phi_1 - \Phi)}\, e^{j2\pi k \frac{d \cos \alpha_2}{\lambda}} \quad (5)$$

where superscript m signifies multipath.

α_1 = elevation angle of the direct signal,
α_2 = elevation angle of the indirect signal,
Φ = phase difference at the target* between the direct and reflected waves. (It is the sum of the reflection coefficient phase-angle ϕ and a phase difference β that results from the path length difference δ between the direct and reflected rays),
ρ = the magnitude of the reflection coefficient, and
= $\rho_o\rho_s$
ρ_o = smooth sea reflection coefficient
ρ_s = specular scattering coefficient
ϕ_1 = arbitrary phase constant
D = divergence factor due to curvature of the earth.

In Eqn. (5) it is assumed that the angular separation of the two signals is small compared to the elemental antenna beamwidths so that the antenna gain is constant for the two signals. In practice, this is a good assumption because the elemental artenna beamwidths are about 10 degrees and the direct and indirect signals arrive near antenna boresight with a separation of only a fraction of a degree. Other simplifying assumptions used in deriving Eqn. (5) are: (i) noise is negligible, (ii) reflection takes place from a smooth sea surface, and (iii) the individual wave fronts are planar. In reality the sea is seldom perfectly smooth, and the multipath model used in deriving Eqn. (5) is complicated by signals scattered from waves on the sea surface which add incoherently at the radar antenna. In practice, it is assumed that this results in diffuse multipath which has the characteristics of noise and can be processed using filtering techniques.

Eqn. (5) uses the plane-wave approximation derived from the more exact geometric optics interpretation of multipath. The plane wave approximation assumes that the wavefront of the two signals are essentially planar, therefore, each will produce a linear phase distribution along the receive aperture. To determine whether the wave

---

*The discussion is limited to one-way propagation, i.e. CHA tracking using beacons. When formulating an equation analogous to Eqn. (5) for two-way propagation, one must take account of the modulation of signal amplitude at the target due to interference between the direct and indirect signals arriving from the radar.

fronts can be treated as being linear or whether corrections have to be made for wave curvature, the following factors must be considered: (a) target range, (b) aperture size, and (c) the requirements of phase accuracy. The Sagitta equations [6] from optics can be used to determine the linearity of a wave front, i.e.

$$d = \frac{r^2}{2R} \tag{6}$$

where d = departure of the wave front from linearity,
r = displacement at right angles to the ray path, and
R = range.

Eqn. (6) can be easily modified to express the departure of a wave front from linearity in terms of phase, giving

$$\varphi = \frac{\pi r^2}{\lambda R} \quad . \tag{7}$$

As an example of the use of Eqn. (7), if $R = 5000$ m, $\lambda = 0.032$ m and a phase accuracy of 1 degree is required, the maximum aperture size one can use without making corrections for curvature is 0.943 m.

Returning to Eqn. (5) it can be rearranged into the following form

$$s_k^m = \underbrace{f(t-\tau_r)\, e^{j(2\pi f_d t + 2\pi k \frac{d\cos\alpha_1}{\lambda} + \phi_1)}}_{\text{Amplitude - Doppler}} \underbrace{\{1 + \rho D e^{j[\frac{2\pi kd}{\lambda}(\cos\alpha_2 - \cos\alpha_1) - \Phi]}\}}_{\text{Interference Pattern}} \quad . \tag{8}$$

As shown, Eqn. (8) consists of two factors, one describing target cross-section, an unknown phase ϕ_1 and velocity, and the other the multipath interference pattern. The latter is a function of the angular separation of the direct and indirect signals and also their phase difference, Φ, at the reference element. The information contained in the Amplitude-Doppler term is not used in CHA processing. However, it can be indirectly useful if it makes coherent integration possible, wherein the SNR of the radar signal is enhanced prior to CHA processing. Since CHA is a multipath processor, it only makes direct use of the interference pattern term in Eqn. (8).

The Interference Term

A graphical interpretation of the interference term in Eqn. (8) is given in Figure 4 [7]. This figure shows the spatial standing wave pattern which results from interference between two waves propagating in space, whose ray separation angle is 2α. The x-y plane in Figure 4 is defined as the plane generated by the two vectors in the direction of propagation of the two interfering plane waves. The characteristics of the standing wave pattern are given in terms of equiphase surfaces and loci of the maxima and minima of the resulting amplitude. The parameter h is the ratio between the amplitudes of plane wave no. 1 and 2. Two limiting cases and an intermediate case of h are shown. For h=0, this reduces to the single plane wave case with the constant phase loci defining a plane (or a line on the x-y plane). For h=1, the constant phase loci are seen to be a set of parallel planes with periodic discontinuities in y. The period and the size of these discontinuities are functions of α. For intermediate values of h (e.g., h=0.5 in Figure 4) the constant phase loci on the x-y plane resemble a set serpentine curves, with sharp periodic shifts in the x-direction. The dash curves represent the family of constant phase loci for various values of phase angles.

It is these characteristic constant-amplitude and constant-phase loci which give rise to the superresolution capability of the CHA algorithm. In the multipath case the two waves are the direct and indirect waves. To derive the phase and amplitude distribution of the interference pattern across a particular aperture, one must take into account the angular separation of the two signals in addition to the orientation of the aperture with respect to the signal rays.

Figure 5 gives an example of an interference pattern measured at the Ottawa River [8] using a vertical receiving antenna with an aperture of 17.2m. Theoretically derived results are superimposed for purposes of comparison with reasonably good agreement. In this example the range is 5500m, source height is 5.5m and the height of the centre of the receiving antenna is 12.3 m. In terms of Figure 4, both the direct and indirect rays arrive near boresight, but with a slightly negative (downward) tilt. The tilt of the indirect ray will be slightly greater than that of the direct ray. Since the rays are fixed in this diagram let us tilt the antenna to approximate the angles of arrival of the two rays with respect to the antenna boresight. The antenna in Figure 4 would be represented by a straight line with a slightly negative tilt with respect to the axis shown. As one traces along this line, the phase decreases very slowly in a monotonic fashion until it approaches a point near a null of the interference pattern where the phase front is corrugated. This occurs at a height of 16.5 m in Figure 5. Minima are usually marked by a phase reversal followed by a rapid decrease, all in quick succession. Following the minimum the trace returns to a slow monotonic decrease.

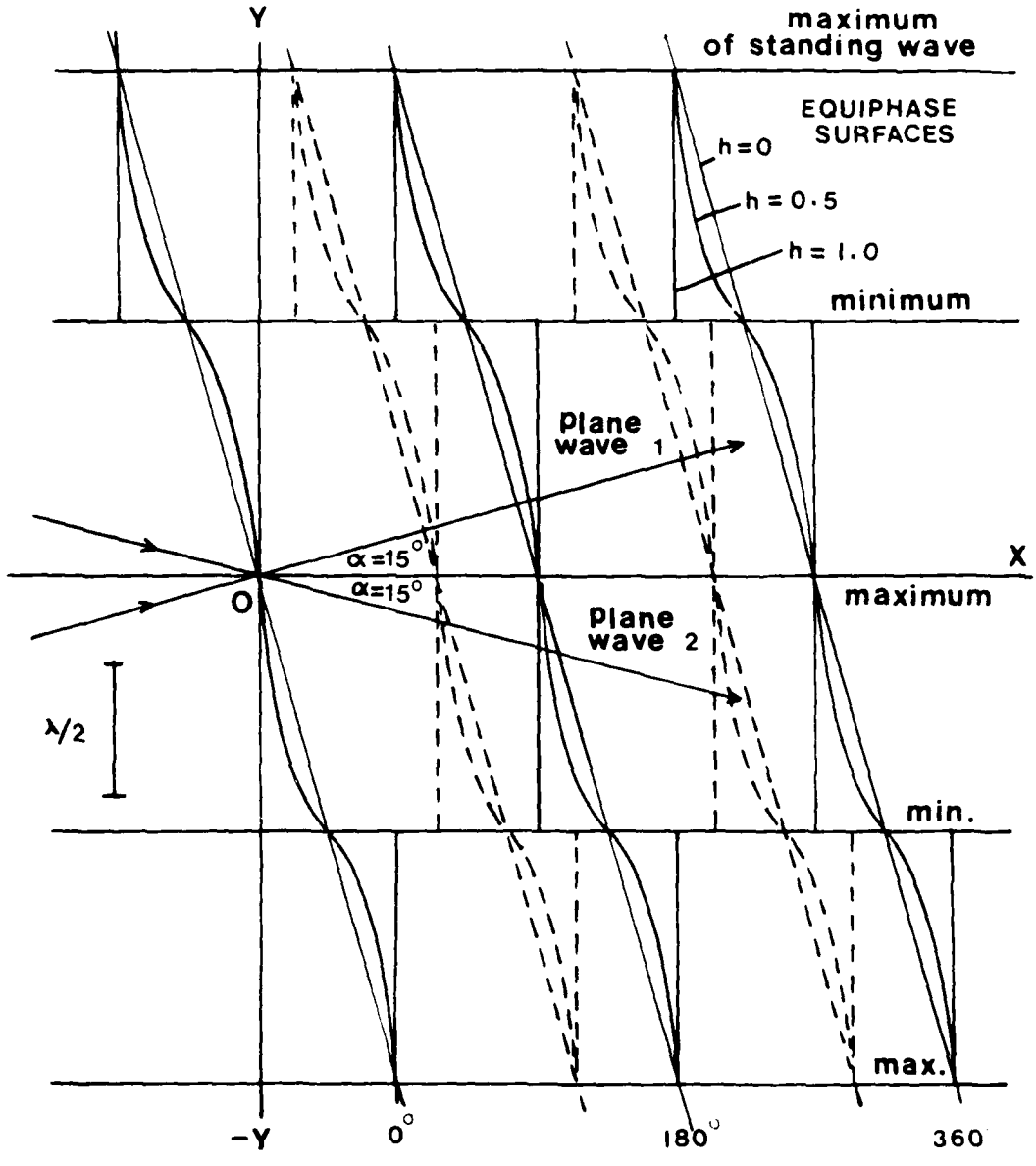

$$Y = \frac{-\lambda}{2\pi \sin\alpha} \text{ ARC TAN } \left[\frac{1+h}{1-h} \text{ TAN } \left(\frac{2\pi \times \text{COS } \alpha}{\lambda}\right)\right] - \frac{n\lambda}{\sin\alpha}$$

$$n = \cdots -3.\ -2.\ -1.\ 0.\ +1.\ +2. \cdots \qquad h = \frac{\text{AMPLITUDE OF RAY 2}}{\text{AMPLITUDE OF RAY 1}}$$

Figure 4 - Wave Interference Pattern for Ray Separation 2α

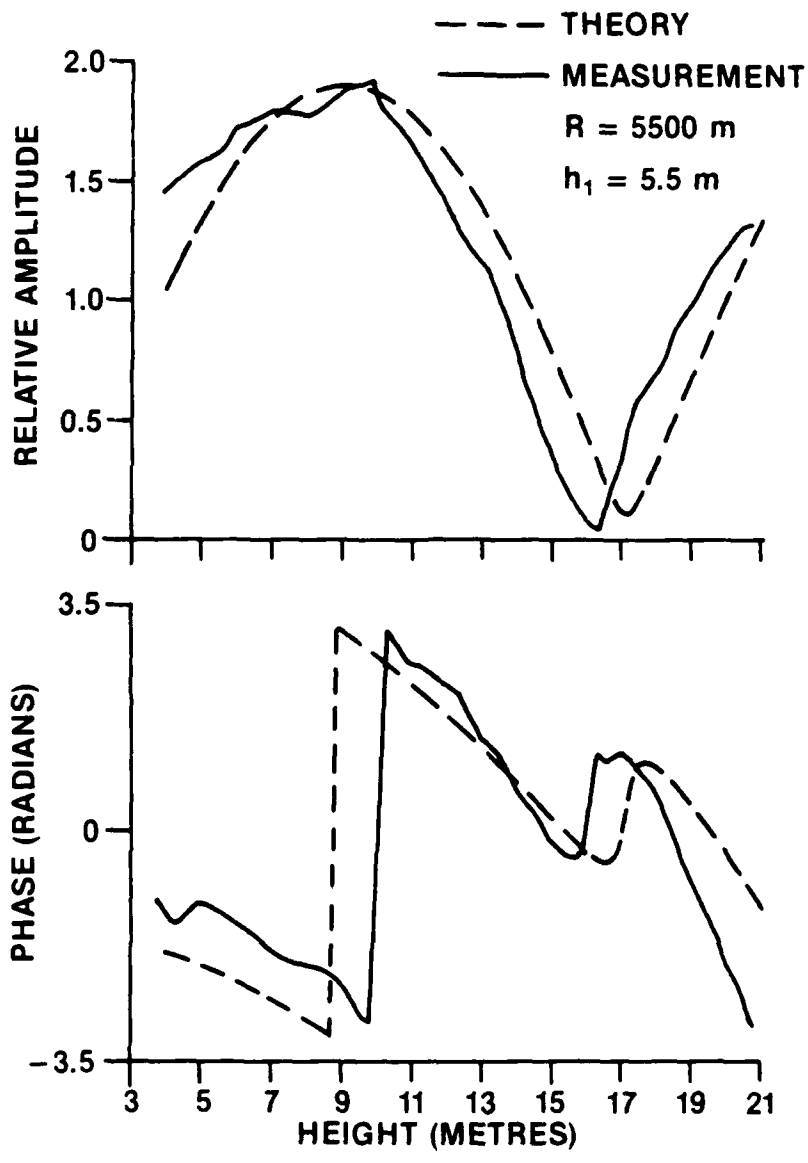

Figure 5 - Amplitude and Phase Interference Patterns for Range 5500 m and Target Height 5.5m

3. CHA-SAMPAR SYSTEMS

3.1 CHA in Conventional SAMPAR

Equation (8) forms the basis for CHA processing of multipath data recorded with a conventional coherent SAMPAR system. This equation gives the radar signal following synchronous detection. As it stands it is not suitable for CHA processing on two counts. First, it is a function of target cross section and second it is a function of target velocity. In order to eliminate the dependence of the amplitude on target cross section this equation can be normalized with respect to the signal at the reference element (k=0):

$$s_o^m = f(t-\tau_r)\xi\, e^{j(2\pi f_d t + \phi_1 + \phi_2)} \tag{9}$$

where $\xi = \sqrt{1+2D\rho\cos\Phi + D^2\rho^2}$,

$$\phi_2 = \tan^{-1}\left[-\frac{D\rho\sin\Phi}{1+D\rho\sin\Phi}\right]$$

and subscript m signifies multipath signal giving

$$s_{kn}^m = \frac{1}{\xi} e^{j(2\pi k \frac{d\cos\alpha_1}{\lambda} - \phi_2)} \left\{1 + D\rho e^{j[\frac{2\pi kd}{\lambda}(\cos\alpha_2 - \cos\alpha_1)-\Phi]}\right\}. \tag{10}$$

The second subscript, n, indicates normalization with respect to the reference channel. Equation (10) is now suitable for CHA processing because it is a function only of the angle of arrival, range, reflection coefficient and divergence coefficient, all of which can either be measured directly or can be modelled.

An independent estimate of target height can be made by CHA processing which involves only the aperture samples at a single discrete time instant. If the signal-to-noise (SNR) ratio is sufficiently high, then there is no coherence requirement among consecutive aperture sample sets. In practice, however, some integration is required to enhance the SNR.

3.2 CHA in Self-Cohering SAMPAR

3.2.1 Examples of Self-Cohering SAMPAR Systems

Although operational radar systems do not use self-cohering techniques to maintain phase coherence, there is a role for such systems. For

the most part, this is restricted to test ranges. In this application, they are used for collecting data to test new subsystems or algorithms for predicting radar performance. It is worthwhile therefore to describe these systems, even if only briefly. This is particularly true when one considers that self-cohering systems were used extensively to develop the CHA algorithm. Following its development, the algorithm was tested with a radar that used a Stalo/Coho and was found to work as predicted.

The CHA development serves as an example of the effectiveness of self-cohering beacon systems using CW signals and one-way propagation for simulating radars. These systems provide data that are comparable with that which would be recorded with a sampled aperture radar, but at only a fraction of the cost. Under these conditions, reasonably high SNRs can be realized, simply by using beacons with sufficiently high powers.

An example of a self-cohering system is the Ottawa River Low-Angle Tracking Range [8]. This facility has been used by CRC to develop and test low-angle tracking algorithms, particularly the CHA algorithm. As well, it has been used to collect data to determine the effects of anomalous propagation on low-angle tracking algorithms.

A diagram of the Ottawa-River Facility is given in Fig. 6. It consists of two self-cohering SAMPAR systems. One is a two-element system, consisting of a reference and a coherent-antenna/receiver. This system is called a vertical profiler. Aperture sampling is carried out in a serial fashion and occurs as the trolley moves along the tower. The other is a conventional 8-element array system, with an aperture of one metre. The aperture sampling in this case is carried out in a parallel manner. Of the two systems, the 8-element one is nearest to what an operational radar might look like. At least, its aperture is comparable to that of conventional systems.

Figure 7a gives a picture of the Ottawa River Low-Angle Tracking Range. The locations of both the vertical profiler and the 8-element SAMPAR systems are identified in the picture. As well, Figure 7b gives a picture of the 8-element array. Here we see the antenna elements and the corresponding receivers.

The profiler is a large aperture SAMPAR system with an effective aperture of 17 m. The resolution of the profiler as given by $0.88\lambda/L$ is equal to 1.4 mrad or 0.081 degrees. In addition to measuring angles-of-arrival of the direct and indirect signals in Fig. 6, the profiler measures the tropospheric refractive index gradient. This is achieved by equipping the trolley, which carries the coherent receiver, with meteorological sensors for measuring temperatures, relative humidity and pressure. From these meteorological data one is able to derive the refractivity gradient. This allows the profiler to be used for correlation studies between angle-of-arrival deviations and refractivity gradients.

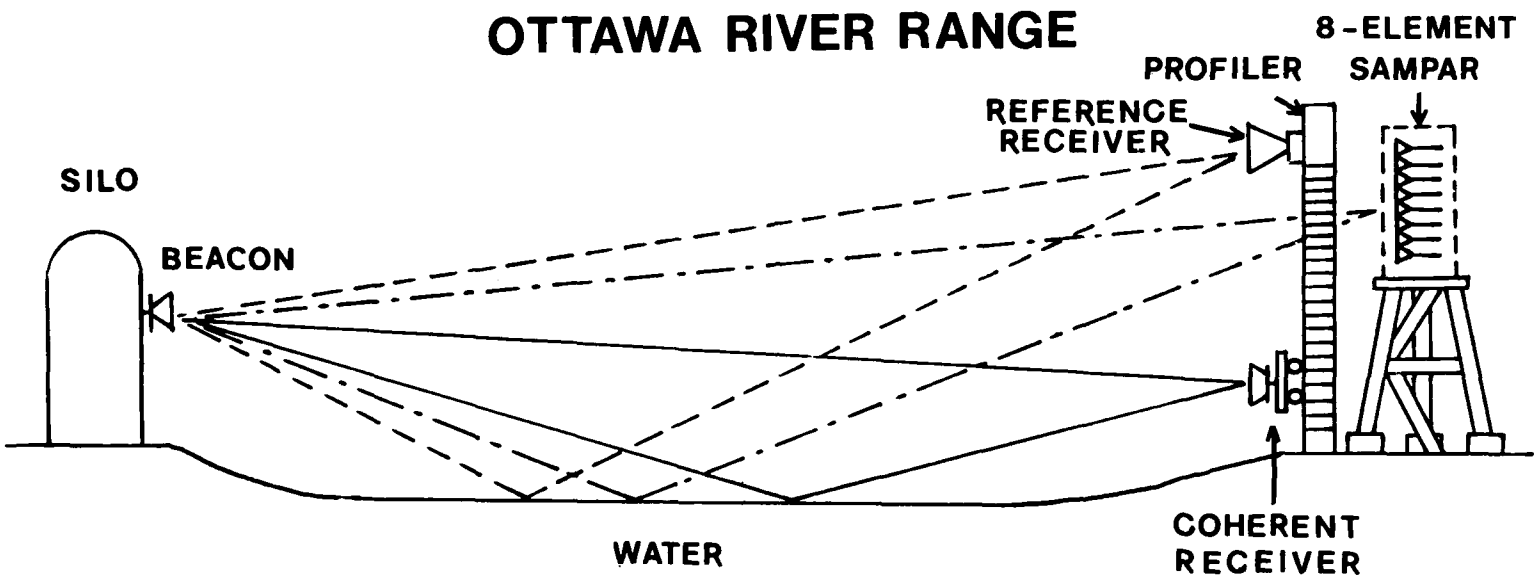

range = 13530 m

beacon height = 18 m

reference-receiver height = 19.1 m

coherent-receiver height = 3.7 To 20.9 m

Figure 6 - Ottawa River Low-Angle Tracking Range
with Some Geometrical Parameters.

Figure 7a - Ottawa River Low-Angle Tracking Range

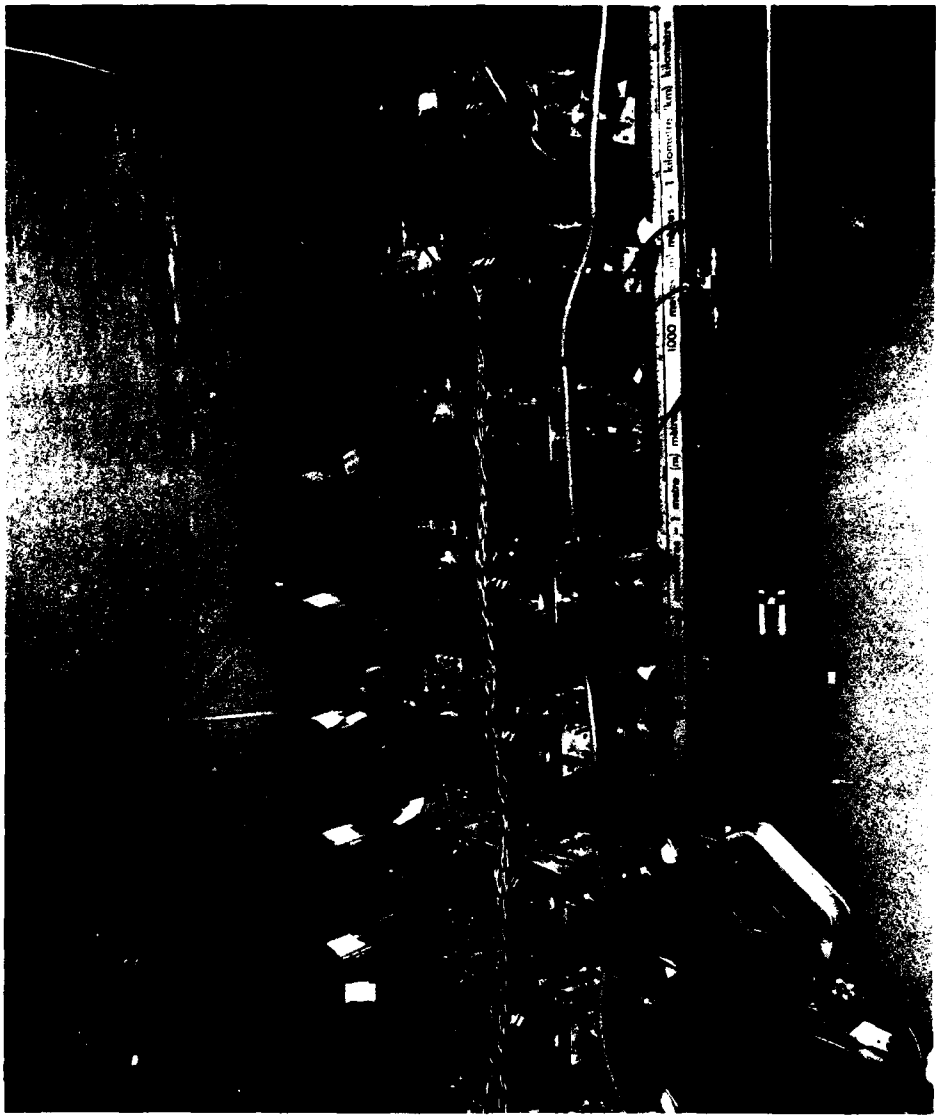

Figure 7b - Eight-Element SAMPAR System

In both cases, the first local oscillator (LO) in each system is common to all of the elements of that system. The profiler has only two elements, whereas the array system has eight elements. Again in both systems the second LO, rather than being derived from a stable oscillator, is derived from the signal arriving at one of the elements. This signal is obtained from the reference receiver in the case of the array antenna. There is some advantage to be gained by deriving the array reference signal by combining all of the element signals. This provides some measure of protection against the eventuality of a null in the interference pattern coinciding with the reference element, thereby degrading the quality of the reference signal. If a null coincides with the reference antenna in the case of the profiler, the system signals can be seriously degraded. This degradation can only be overcome by moving the reference antenna or by having a second reference antenna which is spatially separated from the first.

3.2.2 Multipath Signals in Self-cohering CHA-SAMPARS

CHA processing is possible using signals from any SAMPAR system in which the multipath interference-pattern information is preserved. If a self-cohering system is used, the appropriate form of Eqn.(8) becomes:

$$s^m_{kd} = \frac{f^2(t-\tau_r)}{2} e^{j2\pi\frac{kd\cos\alpha_1}{\lambda}} \{1 + \rho D\, e^{j[\frac{2\pi kd}{\lambda}(\cos\alpha_2-\cos\alpha_1)- \Phi]}$$

$$+ D\rho\, e^{j\Phi} + D^2\rho^2 e^{j\frac{2\pi kd}{\lambda}(\cos\alpha_2-\cos\alpha_1)}\} \qquad (11)$$

If α_1 and $\alpha_2 \approx \pi/2$ then $\cos\alpha_1 \approx \pi/2-\alpha_1$, and $\cos\alpha_2 \approx \pi/2 - \alpha_2$. With these approximations Eqn. (11) becomes

$$s^m_{kd}(t) = \frac{f^2(t-\tau_r)}{2} e^{j2\pi\frac{kd\cos\alpha_1}{\lambda}} \{1 + D\rho\, e^{j[\frac{2\pi kd}{\lambda}(\alpha_1-\alpha_2)- \Phi]}$$

$$+ D\rho\, e^{j\Phi} + D^2\rho^2 e^{j[\frac{2\pi kd}{\lambda}(\alpha_1-\alpha_2)]}\} \,. \qquad (12)$$

Eqn. (12) is still not in a form suitable for CHA processing because of its dependence on $f(t-\tau_r)$. A dependence on parameters such as target cross section and transmitted power is undesirable because the results obtained from signal processing of the radar signal are a function of target cross section which is usually unknown. Therefore, Eqn.(12) is normalized using:

$$s_{od}^{m}(t) = \frac{f^2(t-\tau_r)}{2}(1 + 2\,D\rho\cos\Phi+D^2\rho^2) \qquad (13)$$

which is the signal from the reference antenna, giving the result

$$s_{kd}^{m}(t) = \frac{e^{j\frac{2\pi kd\cos\alpha_1}{\lambda}}}{(1+2D\rho\cos\Phi+D^2\rho^2)}\{1 + D\rho e^{j[\frac{2\pi kd}{\lambda}(\alpha_1-\alpha_2)-\Phi]}$$

$$+ D\rho\, e^{j\Phi} + D^2\rho^2 e^{j\frac{2\pi kd}{\lambda}(\alpha_1-\alpha_2)}\} \; . \qquad (14)$$

The expression in the brackets is the interference term which is a strong function of the differences in both the elevation angles and phases of the direct and indirect signals. It is a weak function of the reflection coefficient and the divergence. Because of normalization the amplitude term which modulates the interference factor is now independent of target cross section and the radar's parameters.

The advantages of a self-cohering SAMPAR are its basic simplicity, leading to lower costs, and the fact that correcting circuitry is not required for LO instabilities because of an inherent self-correcting feature. Because of this feature, Eqn. (14) need not be modified to account for LO frequency drift. Costs are less, compared to a conventional SAMPAR, because there is no need for a Coho and Stalo in a self-cohering system.

The major disadvantage of a self-cohering system lies in the quality of the reference signal used for synchronous detection. Since the reference signal is derived from the received beacon signals it can be degraded by system noise and interference, i.e. its SNR is usually less than that for the case of a conventional system. In a conventional system, the reference signal is derived from signal generators and therefore is consistently of high quality. For this reason a self-cohering system is never used in an operational radar.

3.3 Doppler Processing and Coherence Consideration in SAMPAR Systems

a) Doppler Processing in a CHA-SAMPAR System

Shipborne radars must be able to operate in heavy sea-clutter environments. These include both surveillance as well as fire-control radars. If the single-pulse sensitivity of the radar is not sufficient to permit the detection of targets, some form of integration is performed in order to enhance the signal-to-noise ratio. In most cases, coherent integration of contiguous radar returns is required.

In a practical SAMPAR employing CHA processing, Doppler processing is required for clutter suppression. Doppler processing is a form of coherent integration used in radar applications to extract weak target signals from background clutter and noise. Because target velocity is usually unknown, integration in a coherent system is best realized using temporal Fourier (Doppler) processing. Fourier processing in the digital domain is accomplished using the DFT or the FFT. The DFT is defined as:

$$X(m) = \frac{1}{N} \sum_{k=0}^{N-1} x(k)\, e^{-j2\pi mk/N} \qquad (15)$$

$$k=0,1,2,\ \ldots,N-1$$
$$m=0,1,2,\ \ldots,N-1$$

The DFT can be viewed in a number of ways depending on the processing that follows it. For example, it can be thought of in terms of a correlation between the signal being processed and sinusoids of known frequencies. From this point of view, the magnitude of the cross-correlation function is a measure of the spectral contents of the unknown signal. Alternatively, Fourier processing can be thought of in terms of bandpass filtering. Now we think of the DFT as a bank of N bandpass filters whose bandwidths are given by 1/NT, where N is the number of samples and T is the sample spacing. Either of these interpretations will be useful for the discussion being entered into here.

After coherent demodulation and sampling in the complex base-band, the time series representing the returns from a moving target is given by:

$$x(k) = f(t-\tau)e^{j\left(\frac{2\pi f_D k}{N}\right)} \qquad (16)$$

Figure 8 depicts a typical SAMPAR system employing CHA processing. Each element of a linear array has its own coherent receiver, which converts the received signal down to complex video domain. The signal from each channel is then sampled by an analog-to-digital converter (ADC). Each complex sample represents the return of the transmitted pulse from a particular range gate. As successive pulses are transmitted and received, the samples from a given range gate for each pulse will form a time series representing the returned signal of the pulse train from that particular range gate. This time series is passed through a moving target indicator (MTI) filter in order to suppress the sea-clutter component. The MTI filter is usually a complex non-recursive digital filter composed of unit delays and complex coefficients, such as the one shown in Figure 9. The filter coefficients are designed to place an appropriate stop band in a region of Doppler frequencies where the sea-clutter spectrum is located. The MTI filter effectively removes most of the sea-clutter energy in the signal and minimizes any sea-clutter residues which could leak, through the subsequent DFT operation, into the spectral region where the target might be located. In order to maximize the SNR, the MTI filtered time series is passed through an FFT. The dimension of the DFT,

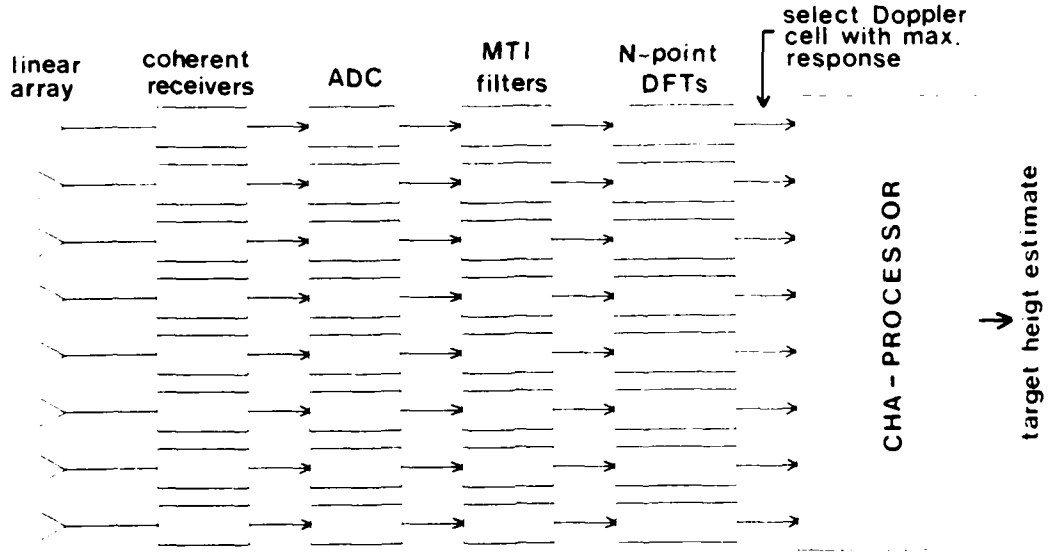

Figure 8 - A typical SAMPAR system empliying CHA processing

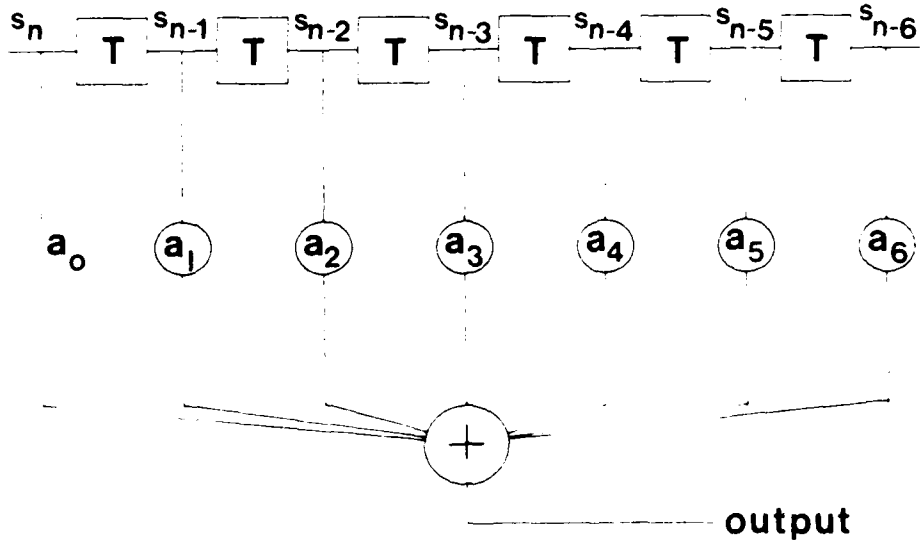

Figure 9 - A 6-Stage Finite Impulse Response Filter.

N, should be large enough to process the output time series from the MTI filter. Since for a non-recursive filter, steady state is reached after all the unit delays are filled (see Figure 9), N is equal to the difference between the length of the input time series and the number of unit delays in the non-recursive MTI filter. However, due to practical constraints such as processing speed and coherence limitations, a DFT of smaller dimension may be used. This, however, means that only a fraction of the MTI-filtered samples are used, and therefore the maximum SNR is not realized. For an N-point DFT, there are N output samples, each representing the spectral power of one of N regions equally dividing the Doppler band. If the target signal has sufficient energy to be detected, its energy will be concentrated in the Doppler cell whose frequency matches most closely that of the target Doppler. The MTI filtering and DFT are performed for all the channels of the SAMPAR systems. For each pulse train, there will be a set of Doppler-processed aperture samples with enhanced SNR. This set of aperture samples is then fed to the CHA processor for target height estimation. The details of the CHA processor is explained elsewhere [4] and will not be repeated here.

Assuming that the target Doppler frequency matches one of the frequency cells of the DFT, say the mth cell, the output of this frequency cell in reponse to a signal in Eq. (8) is given by:

$$s_k^m(t) = Nf(t-\tau_r)e^{j(2\pi k\frac{d\cos\alpha_1}{\lambda} + \phi_1)} \left\{1 + D\rho\, e^{j[\frac{2\pi kd}{\lambda}(\cos\alpha_1-\cos\alpha_2)-\Phi]}\right\}, \quad (17)$$

Normalizing with respect to the reference element k=0 using

$$s_o^m(t) = Nf(t-\tau_r)\,\xi\, e^{j(\phi_1 + \phi_2)} \quad (18)$$

where ξ is as defined in Eq.(9)

Eqn. (17) becomes

$$s_{kn}^m(t) = \frac{1}{\xi} e^{j(2\pi k\frac{d\cos\alpha_1}{\lambda} - \phi_2)} \left\{1 + D\rho e^{j[\frac{2\pi kd}{\lambda}(\cos\alpha_2 - \cos\alpha_1)-\Phi]}\right\} \quad (19)$$

which is equivalent to Eqn. (10), except for the fact that the SNR is increased by a factor of N because of temporal integration. (This would be apparent in a development that included system noise, in that the noise will be reduced by the factor N).

In the worst case, the target velocity may correspond to a Doppler frequency which is mid-way between two Doppler cells. The SNR improvement would be about 3.9 dB less due to the roll-off in the FFT response.

Doppler processing can be carried out provided that the following requirements are met, a) the target remains in the same range cell throughout the time interval of the pulse train, and b) phase coherence is maintained over the coherent integration interval.

In reality, however, moving targets will migrate to neighbouring radar resolution cells. Thus the coherent integration time is limited by the target velocity and the range resolution of the radar.

Figure 10 compares the maximum time a target remains in a range cell as a function of target speed for two range cell resolutions. (The radar frequency is assumed to be 9.6 GHz, corresponding to a wavelength of 3.125 cm.) For a 1 microsecond pulse width (150 m range resolution), it would take a mach 1 target about 455 msec to traverse a range cell. Assuming a PRF of 5 kHz, over 2000 samples may be coherently integrated. On the other hand, it would only take 45 msec for the same target to traverse a 15 m range cell. This assumes the target is at the far side boundary of the range cell at the start of sampling. In this case, the number of samples which can be coherently integrated is about 200.

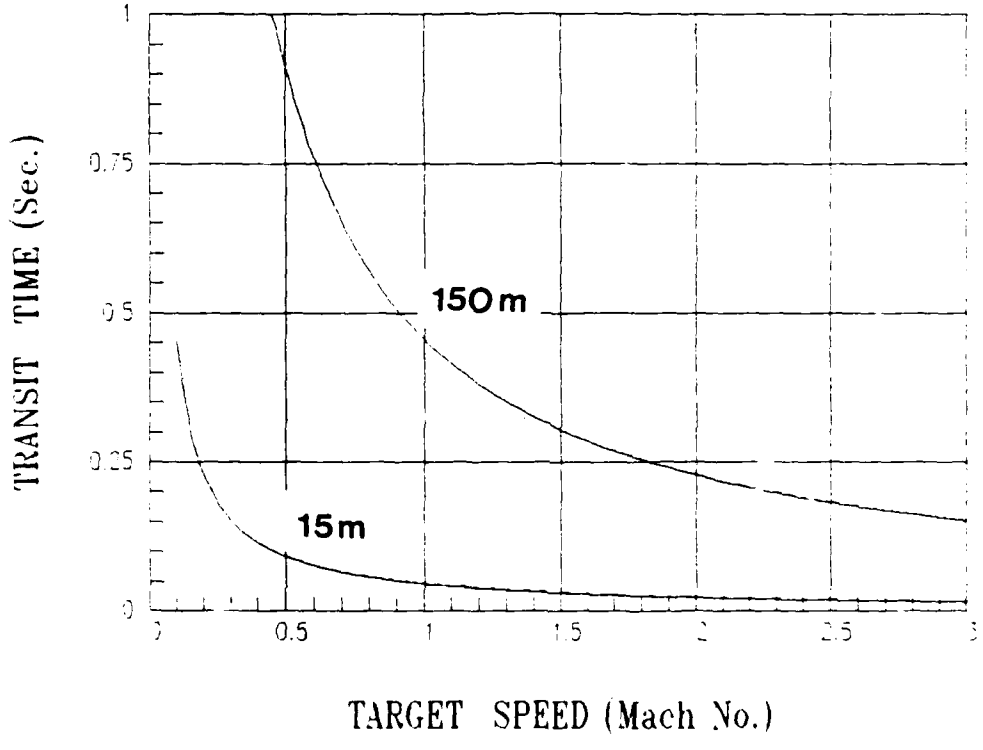

Figure 10 - Transit time for targets of various speeds for two range resolutions.

b) Coherence Considerations for CHA-SAMPAR Systems

Signal coherence in a CHA-SAMPAR system arises as a result of MTI filtering and Doppler processing requirements. Degradation in coherent integration is a consequence of system instabilities. These instabilities come from the STALO and COHO, from the transmitter pulse-to-pulse frequency or phase change, from the inability of the COHO to lock perfectly to the phase of the reference pulse, and from timing and amplitude jitter on pulses. Of these sources of system coherence degradation, STALO stability and COHO locking accuracy are the most difficult requirements to meet.

Harris [9] reports that the US Navy has found the Mark 92 fire-control radar to have poor performance because of rain clutter. The US Navy attributes this to the poor stability of the magnetron and also because the frequency of a magnetron transmitter varies slightly from pulse to pulse. To remedy the problem, crystal-controlled frequency synthesized exciters and TWT power amplifiers have been installed. The higher average power provides some range extension and resolution is maintained, or improved, by pulse compression.

Random system instabilities pose serious problems for coherent integration. These instabilities place a limit on the realizable coherent integration gain as well as MTI performance. A figure of merit commonly employed in measuring MTI systems is the improvement factor defined as the ratio between the output signal-to-interference ratio of the system. The limitations on the attainable MTI improvement factor are summarized in Table 1 [10].

All quantities in Table 1 are peak-to-peak values which occurred on a pulse-to-pulse basis. If it is known that the instabilities are random, the peak values shown in these equations can be replaced by the rms values. For example, if the rms phase change between two contiguous pulses is 0.5°, then the maximum improvement factor is given by

$$20 \log_{10} \left(\frac{1}{.0087266} \right) = 41.2 \text{ dB} \qquad (20)$$

Clutter suppression usiung MTI filters designed for more than 41 dB improvement will not provide additional benefits. Coherent integration can overcome this shortcoming, however, the integration time is limited by the long-term stability of the system, the target velocity and the range resolution.

Table 1: Instability Limitations

Pulse to pulse Instability	Limit on Improvement Factor
Transmitter frequency	$I = 20 \log[1/(\pi\Delta f \tau)]$
STALO or COHO frequency	$I = 20 \log[1/(2\pi\Delta f T)]$
Transmitter phase shift	$I = 20 \log(1/\Delta\phi)$
COHO locking	$I = 20 \log(1/\Delta\phi)$
Pulse timing	$I = 20 \log[\tau/(\sqrt{2}\Delta t \sqrt{B\tau})]$
Pulse width	$I = 20 \log[\tau/(\Delta PW \sqrt{B\tau})]$
Pulse amplitude	$I = 20 \log(A/\Delta A)$

where Δf = interpulse frequency change
τ = transmitted pulse length
T = transmission time to and from target
$\Delta\phi$ = interpulse phase change
Δt = time jitter
$B\tau$ = time-bandwidth product of pulse-compression system ($B\tau$ = unity for uncoded pulses)
ΔPW = pulse-width jitter
A = pulse amplitude, volts
ΔA = interpulse amplitude change

4. SIGNAL-TO-NOISE RATIO CONSIDERATIONS FOR CHA PROCESSING IN SAMPAR SYSTEM

4.1 Signal-to-Noise Ratio

In addition to system losses (including channel mismatch losses), the limit of detection (minimum discernable signal, MDS) for a SAMPAR system operating in a sea environment is set by noise from three main sources. These are the following; (a) back-scatter clutter, (b) forward scatter clutter (sea noise), and (c) system noise. The total noise is given therefore by

$$N_T = N_B + N_F + N_S \tag{21}$$

where N_B = back-scatter sea noise,
N_F = forward scatter sea noise, and
N_S = thermal and receiver noise.

The noise sources identified by Eqn. (21) do not necessarily form a complete list. For example, processing noise, due to quantization and round-off errors is an additional source of noise. For purposes of this report we will restrict the discussion to the noise sources identified by Eqn. (21). Since the received radar signal power is given by

$$S = \frac{P_T G_T G_R \lambda^2 \sigma\, E(n)}{(4\pi)^3 R^4 L_s} \tag{22}$$

where P_T = transmitted power (40,000 w),
G_T = gain of transmit antenna (30.8 dB, 1202.3),
G_R = gain of receive antenna (37.4 dB, 5495.4),
λ = wavelenth (.0313 m),
σ = target cross section(1 m^2),
E(n) = integration gain,
R = range, and
L_S = system loss,

It follows that the SNR for a SAMPAR system operating in a sea environment is

$$SNR = \frac{S}{N_T} M \tag{23}$$

with

$$M = [1 + \rho_o^2 \rho_s^2 + 2\rho_o \rho_s \cos \phi] \tag{24}$$

where ρ_o = smooth sea reflection coefficient,
ρ_s = specular scattering coefficient, and
ϕ = phase between the direct signal and the coherent component of the reflected signal. (It is a function of the low-angle geometry and the modulus of the smooth sea reflection coefficient).

The parameter N_T in Eqn. (23) is somewhat complex and, as indicated in Eqn. (21), consists of three terms.

a) System Noise

The term, N_S is given by the expression

$$N_S = F\ kT\ B \tag{25}$$

where $kT = 4 \times 10^{-21}$ watts/Hz (T=290°K),
B = band width (10^6 Hz) and
F = noise figure (9 dB, 7.943).

The remaining two terms in Eqn. (21), N_B and N_F, result from scattering of the radar signal by a rough sea surface. They are a function of the radar wavelength, the grazing angle and the rms deviation of the sea surface, which is related to sea-state.

Before considering the values of the sea noise terms it is worthwhile considering the frequency of occurrence of sea-state conditions on

the oceans of the world. Sea state is one of the principal parameters which determines the magnitude of the sea noise terms. Some representative results of frequency of occurrence [11] are given in Figure 11, where it is seen that in the Atlantic the probability of the sea-state being greater than SS4 is about 50 percent. On the other hand, for sea-states greater than 5, the probability of occurrence falls to 20 percent.

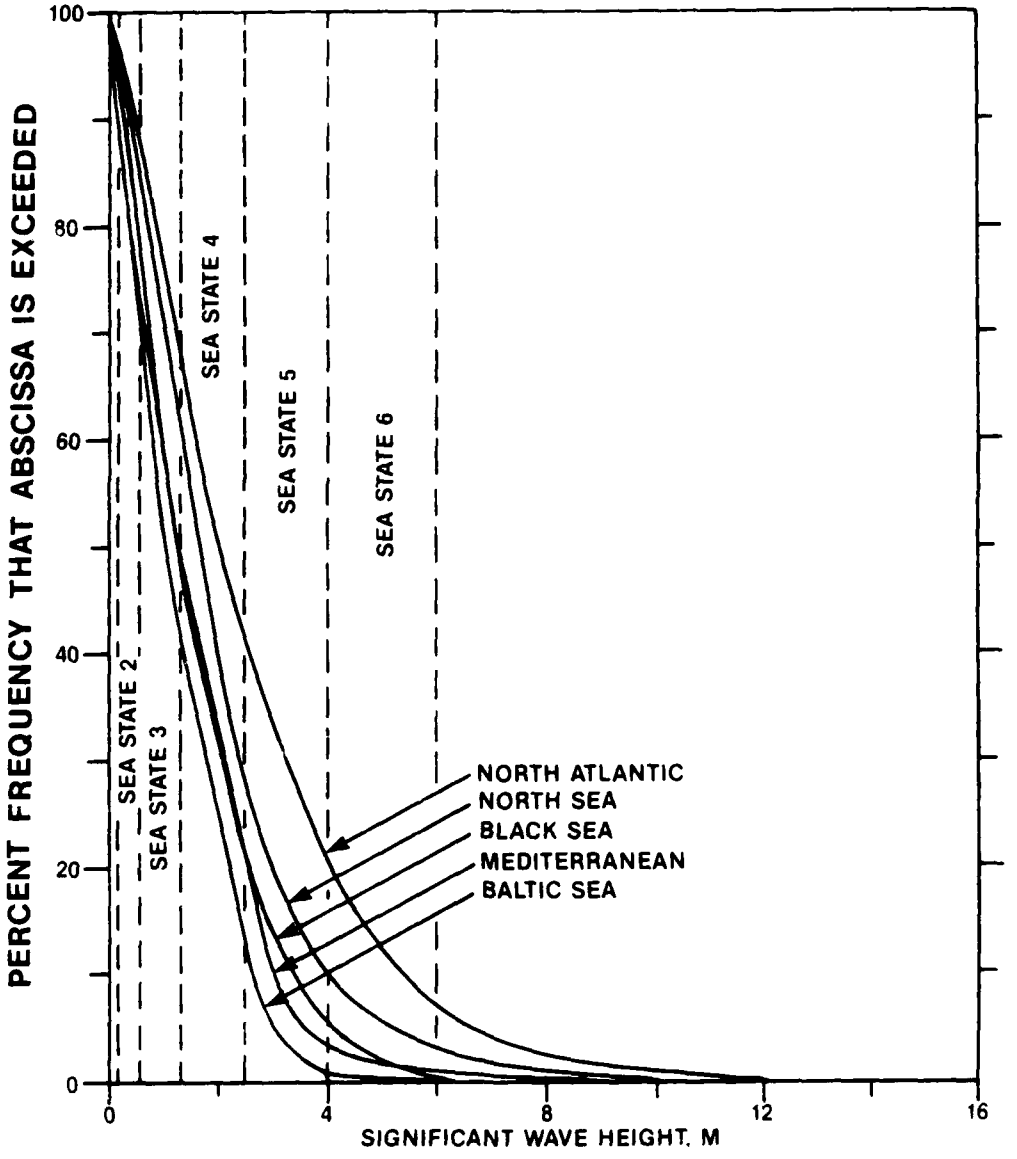

Figure 11 - Comparison of Annual Wave Height Exceedences of Various Locations

b) Backscattered sea noise (radar clutter)

For angles above a critical angle the clutter back-scatter [12] coefficient $\overline{\sigma^0}$ is given by

$$10 \log \overline{\sigma^0} = -64 + 6K_b + 10 \log \text{Sin}\gamma - 10 \log \lambda \qquad (26)$$

where K_b = Beaufort wind scale.

The critical angle is given by

$$\gamma_r = \text{arcsine } (0.066\lambda/\sigma_h) \quad . \qquad (27)$$

Although the roughness parameter is not usually used for back-scatter clutter calculations, it is interesting to note that the critical angle given in Eqn. (27) corresponds to a value of Ψ (66 milliradians) below which experimental results deviate noticeably from the theory. Below the critical angle, the back-scatter coefficient is given by the relationship [12]

$$10 \log \overline{\sigma^0} = \frac{1}{\gamma^2} - 64 + 6K_b + 10 \log (\sin\gamma_r) - 10 \log\lambda - \frac{1}{\gamma_r^2} \quad . \qquad (28)$$

in order to match better the experimental data for medium sea. A broad summary of reflectivity data for both vertical and horizontal polarizations, as compiled by Barton [12] from available sea clutter data, is given in Figure 12 for a medium sea (approximately sea-state 3).

To calculate N_B in Eqn. (21) one has first to derive the sea-surface grazing angle of the radar signal directly below the target. In Figure 13(a) the angle of interest is γ. It is derived from

$$\gamma = \alpha_2 - \alpha_1 \qquad (29)$$

where

$$\alpha_1 = \frac{R}{a - \frac{R^2}{2a}} \qquad (30)$$

and

$$\alpha_2 = \frac{Z_1 + R^2/2a}{R} \qquad (31)$$

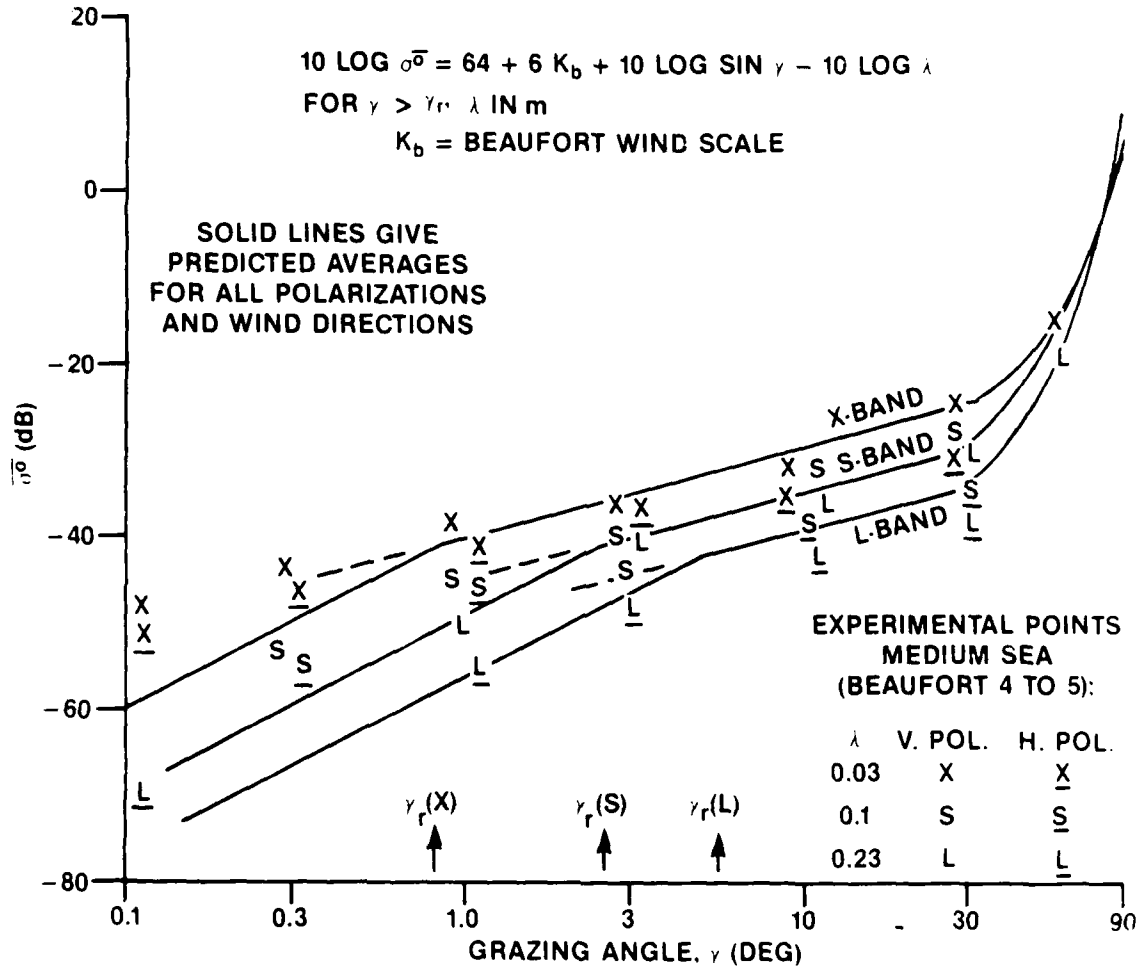

Reprinted, by permission, from D.K. Barton, Radar Clutter, Radars, Vol V, p.58 c 1975 by Artech House, Inc.

Figure 12 - Sea clutter Reflectivity vs Grazing Angle

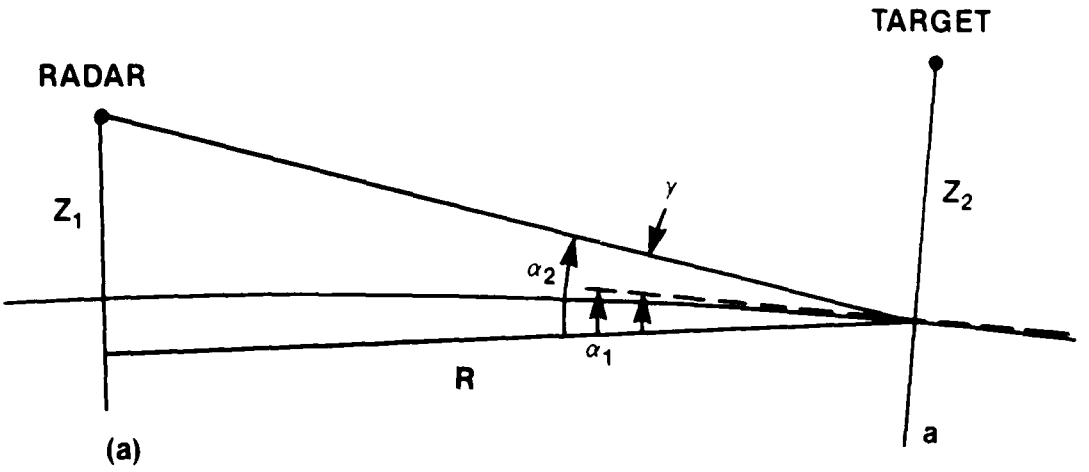

Figure 13a - Backscatter Geometry

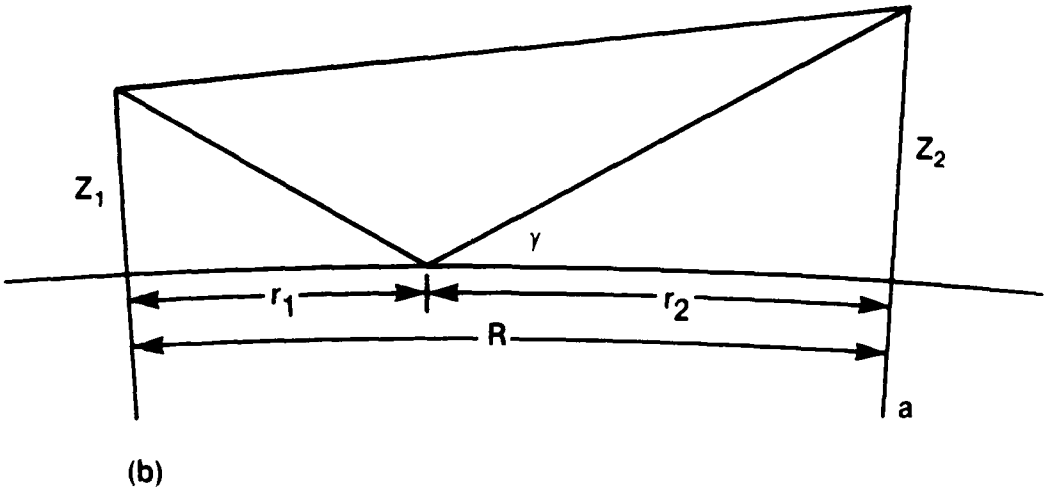

Figure 13b - Forward Scatter and Multipath Geometry

giving

$$\gamma = \frac{Z_1 a - Z_1 R^2/2a - R^2/2 - R^4/4a^2}{R(a - R^2/2a)} \qquad (32)$$

where a = earth's radius.

The effective radar cross section of the clutter is given by

$$\sigma^c = \overline{\sigma^o} \frac{C\tau}{2} R\Theta_B \sec\gamma \qquad (33)$$

Barton [13] writes this equations with a $\sqrt{2}$ in the denominator to take into account the (sinx)/x shape of the antenna beam.

where c = velocity of light,
τ = pulse width, and
Θ_B = 3 dB antenna beamwidth.

The SNR for a 1 m^2 target is derived using Eqns. (22), (26), (28), (32) and (33) and is given in Figure 14 for a number of representative sea-states. A value of Z_1 = 10 m (radar height) was assumed for these results. Superimposed on this figure is a curve giving the SNR for a 1 m^2 target in terms solely of thermal and system noise, where F = 9 DB and B $=10^6$ Hz. The area above the dash curve represents the condition where system noise dominates. In deriving the back-scatter clutter results, the effects of tropospheric refraction were taken into account by replacing the term for the earth's radius in Eqn. (32) with an effective earth's radius given by

$$a_e = ka \ , \qquad (34)$$

where the constant k was derived using

$$k = \frac{1}{1 + \frac{a}{n}(dn/dh)} \ . \qquad (35)$$

In Eqn. (35), n = refractive index
dn = change in refractive index, and
dh = change in elevation.

For a standard atmosphere, k has been determined to be 4/3.

c) Forward Scattered sea noise

The other sea noise component in Eqn. (21), i.e. N_F is derived from the classical scattering theory given by Beckmann and Spizzichino [14]. When a radar signal is reflected from a rough surface the signal consists of two components, one a coherent or specular component and the

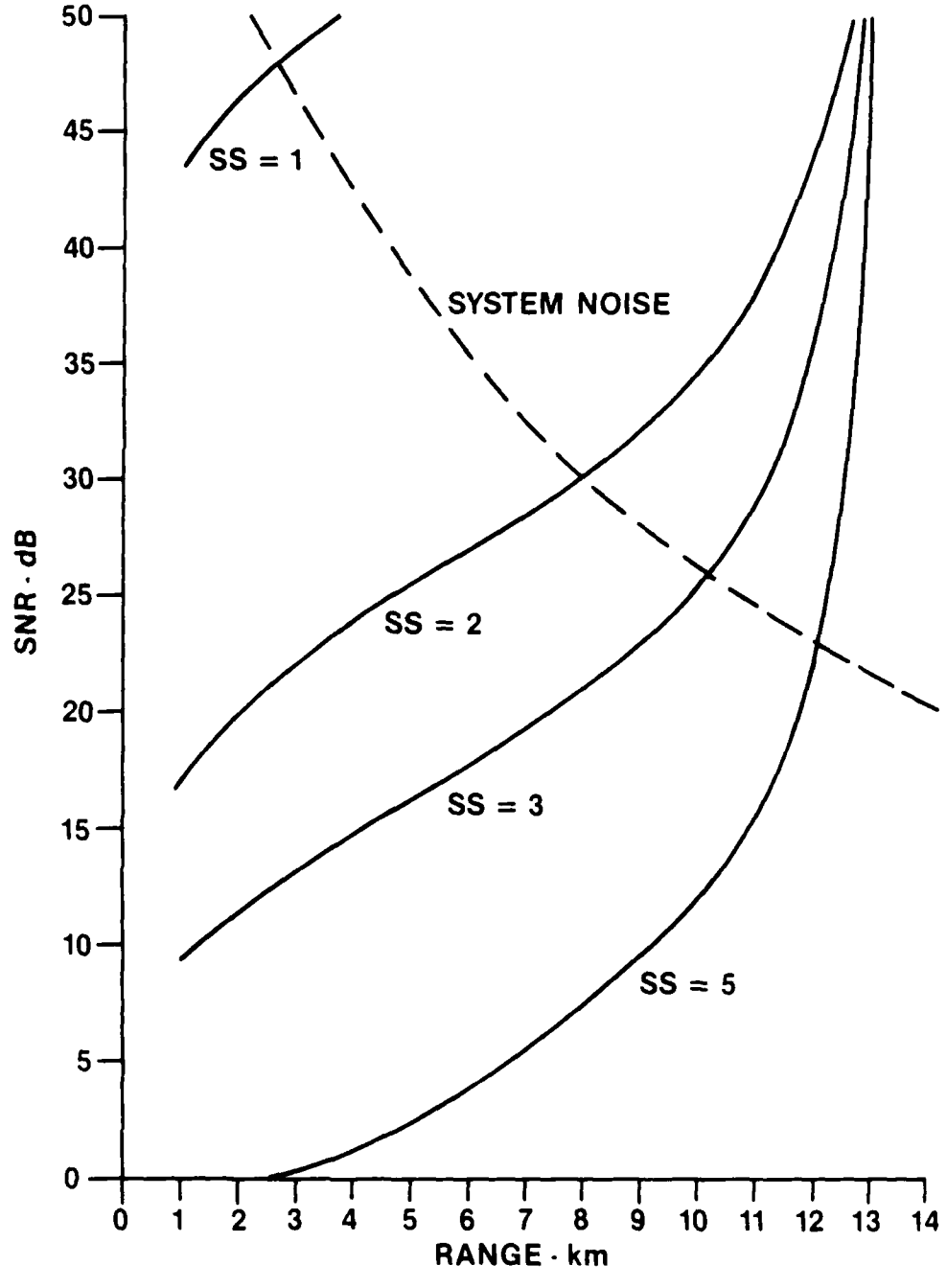

Figure 14 - SNR for $1m^2$ Cross Section Target with Backscattered Radar Clutter

other a random or diffuse component. The signal power is apportioned between these two components in accordance with surface roughness and specular grazing angle. In Figure 15 a comparison of the theory with experimental results obtained by Beard [15]is given. The measurements confirm that the two components exist. The magnitude of the specular component with respect to the direct signal is given by $\rho_o\rho_s$ where ρ is the smooth sea coefficient. Similarly, the magnitude of the diffuse component is given by $\rho_o\rho_d$. Beard's measurements show good agreement with the theory, except for values of ρ_s when Ψ is large. He found that ρ_s did not drop off as quickly as was predicted by theory. For the purposes of this report the experimental branch of the ρ_s curve will be used.

It can be shown [14] that forward scattered sea noise is given by

$$N_F = \frac{2\rho_d^2 \rho_o^2 G_R G_T \lambda^2 \sigma}{(4\pi)^3 R^4} \tag{36}$$

To solve Eqn. (36) for N_F, γ as given in Figure 13(b) must first be derived. This then permits the parameter ρ_d to be obtained from Figure 15. The parameter γ is derived using equations given in Fishback [16]. For example, the range r_1 to the reflection point in Figure 13(b) is given by

$$r_1 = \frac{R}{2} + p \cos\left(\frac{\Phi + \pi}{3}\right) , \tag{37}$$

where

$$p = \frac{2}{\sqrt{3}} \sqrt{a_e(Z_1 + Z_2) + \left(\frac{R}{2}\right)^2} \tag{38}$$

Eqns. (37), and (38) give the formal solution of the cubic equation

$$2r_1^2 - 3r_1^2 R + [R^2 - 2a_e(z_1+z_2)]r_1 + 2a_e z_1 R = 0 \tag{39}$$

which relates the unknown r_1 and r_2 to the known quantities R, z_1 and z_2 and

$$\Phi = \cos^{-1}\left[\frac{2a_e(Z_2 - Z_1)R}{p^3}\right]. \tag{40}$$

Also based on Fishback [15], the solution is calculated more easily if we introduce the dimensionless distance and height parameters defined as follows:

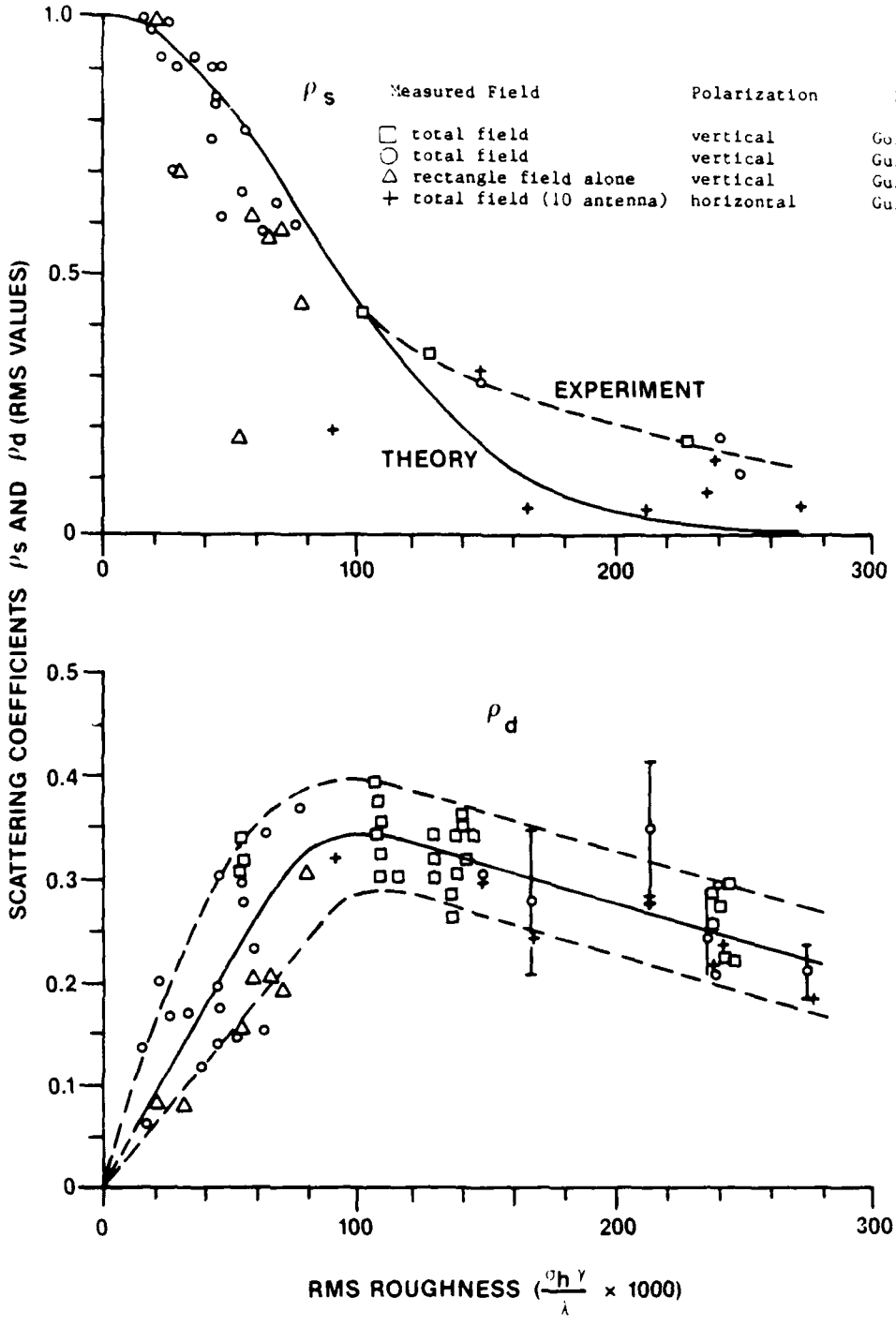

Reprinted, by permission, (copyright © 1978 IEEE), from C.I. Beard, "Coherent and Incoherent Scattering of Microwaves from the Ocean," IRE Trans. on Antenna and propagation, Vol. AP-9, September 1961.

Figure 15 - Specular and Diffuse Scattering Coefficients vs Roughness Compared to Microwave Measurements

$$S_{1,2} = \frac{r_{1,2}}{\sqrt{2a_e Z_{1,2}}} \leqslant 1 \tag{41}$$

$$S = \frac{R}{\sqrt{2a_e Z_1} + \sqrt{2a_e Z_2}} \leqslant 1, \text{ and} \tag{42}$$

$$T = \sqrt{\frac{Z_2}{Z_1}} \leqslant 1, \tag{43}$$

where, in Eqn. (40) Z_2 is taken as the smaller of the two terminal heights in Figure 13(b). Eqns. (41), (42) and (43) are used to determine the following two functions:

$$J(S,T) = (1-S_1^2)(1-S_2^2) \tag{44}$$

and

$$K(S,T) = \frac{(1-S_1^2) + T^2(1-S_2^2)}{1 + T^2} \tag{45}$$

These functions are useful in deriving pertinent equations for a curved-earth geometry from those obtained from flat-earth considerations.

For example, it can be shown that the path length difference between the direct and indirect rays in Figure 13(b) can be approximated by

$$\Delta R = \frac{2Z_1Z_2}{R} J(S,T), \tag{46}$$

and the grazing angle is given by

$$\gamma = \tan^{-1}\left[\frac{Z_1 + Z_2}{R} K(S,T)\right] \tag{47}$$

Using Eqns. (22), (36) and (47), in addition to Figure 15, the SNR for a 1 m^2 target with respect to forward scattered sea noise is derived and presented in Figure 16 for representative sea-states and target heights. Again it is assumed that Z_1 = 10 m. Also, the curve for system noise is superimposed on the results given in Figure 16, as it was for the back-scattered sea noise results in Figure 14.

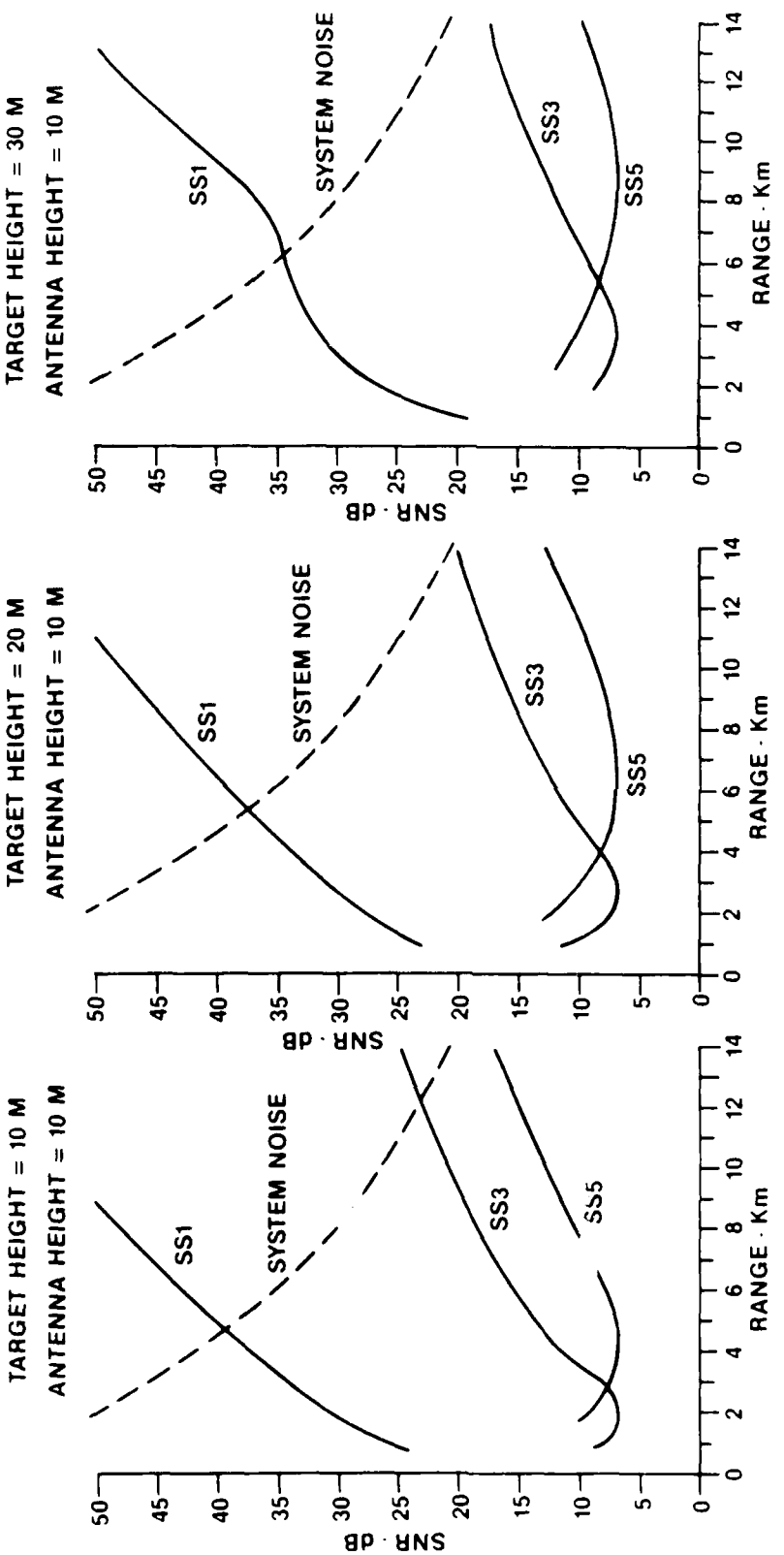

Figure 16 - SNR for forward scattered sea noise

In dealing with forward scattering from a rough ocean it is useful to define an rms roughness parameter, given by

$$\Psi = \frac{\sigma_h \gamma}{\lambda} \qquad (48)$$

where σ_h = rms wave height,
γ = grazing angle, and
λ = wavelength

Because of the importance of the roughness parameter in sea noise calculations, values are given in Table 2 for a number of possible sea-skimmer geometries. It is assumed that SS=4 (i.e. σ_h = 0.5m), radar height = 10 m and λ = 0.032 m. When viewing these results it should be borne in mind that there is an inverse relationship between Ψ and the SNR.

Table 2: Typical values of roughness parameter Ψ (in milli-radians) for sea state 4.

	Range (km)				
Target height(m)	2	5	10	15	20
30	311.3	122.2	57.1	33.4	20.6
20	233.4	91.3	41.9	23.8	13.7
10	155.4	60.2	26.7	13.9	6.44
3	97.8	31.7	3.86		

Some general comments can be made regarding the results given in Table 2. These comments apply to all sea-states. There is a large variation in Ψ due to the wide ranging geometry. Values of Ψ are less for large values of R and smaller values of target height. Of particular note, values of Ψ are usually low for the low target heights that are typical of sea-skimming missiles.

4.2 Multipath SNR Enhancement

The curves for SNR given in Figs. 14 and 16 deal with system noise, back-scattered clutter (sea noise) and forward scattered sea noise. They do not include the effect of the specular component of the reflected signal on the SNR of the Sampar signal. The specular component, whose amplitude relative to the direct signal is $\rho_o \rho_s$, adds vectorially with the direct signal. It can therefore enhance the SNR or degrade it depending on the phase ϕ between the direct and indirect signals. The modulation of the SNR brought about by the coherent component of the reflected signal is given by the second term in Eqn.

(23), i.e. the term identified by M (for two-way propagation the analogous term is given by M^2).

To solve for M, the specular reflection coefficient, ρ_s is obtained from Figure 15 after solving Eqn. (48) for γ. The phase between the direct and indirect signals is given by

$$\phi = -\left[\pi + \frac{4\pi Z_1 Z_2}{\lambda R} \; J(S,T)\right]. \qquad (49)$$

In Eqn. (49) the first term gives the phase shift on reflection, assumed here to be $-\pi$ radians, and the second terms gives the electrical path length difference between the direct and indirect signals multiplied by the propagation constant $(2\pi/\lambda)$. Values for M are given in Figure 17 for SS5 conditions and some typical target heights. Again it is assumed that Z_1 = 10 m. M is seen to take on values ranging from +10 dB to -20 dB. For Z_2 = 10 m, M takes on positive values from at least 14 to 7 km. For lower values of Z_2 the region of positive M extends to even lower values of R.

4.3 Limiting Signal-to-Noise Ratio

In viewing Figs. 14 and 16, it becomes clear that the relative magnitudes of the three dominant noise sources vary with target range, height and sea-state conditions. In other words, if these parameters formed the ordinates of a three dimensional diagram there would be well defined regions in which each would be the dominant noise source. Figure 18 is presented as a final diagram in an attempt to depict these different regions. This figure shows that when SS5 and Z_2 is equal to 10, 20 and 30 m the dominant source of noise is back-scattered clutter for ranges between 0 and 7.7 km. There can be a significant variation in the values calculated for back-scatter clutter, depending on the model used for the sea back-scatter coefficients. For example, the model presented by Abraham [17] predicts the SNR for SS5 as being about 5 dB greater than indicated in Figure 18. With this model, the maximum range for back-scattered clutter would be reduced to about 5.5 km. Beyond 7.7 km, forward scattered sea clutter becomes the limiting noise source for Z_2 = 30 and 20 m, while back-scattered clutter remains the dominant source for Z_2 = 10 m until 10 km. At R = 10 km forward scattered clutter also becomes the dominant noise source for Z_2 = 10 m. For SS3 the dominant noise source is forward scattered sea noise; whereas for SS1 it is split between forward scattered sea clutter and system noise.

5. SUMMARY AND CONCLUSIONS

A review of digital beam forming has been presented from which a definition of spatial frequency evolved. This can be thought of as being

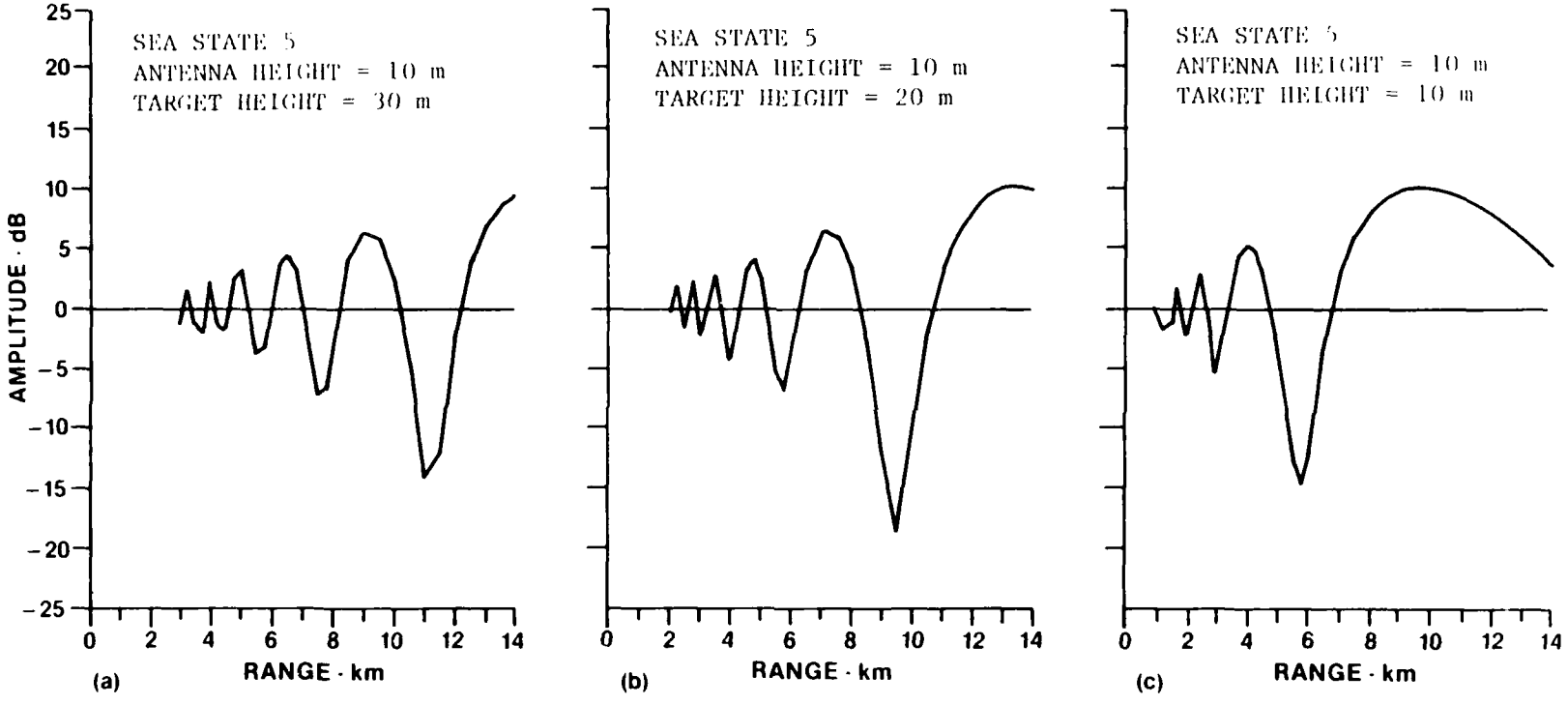

Figure 17 - Multipath SNR enhancement

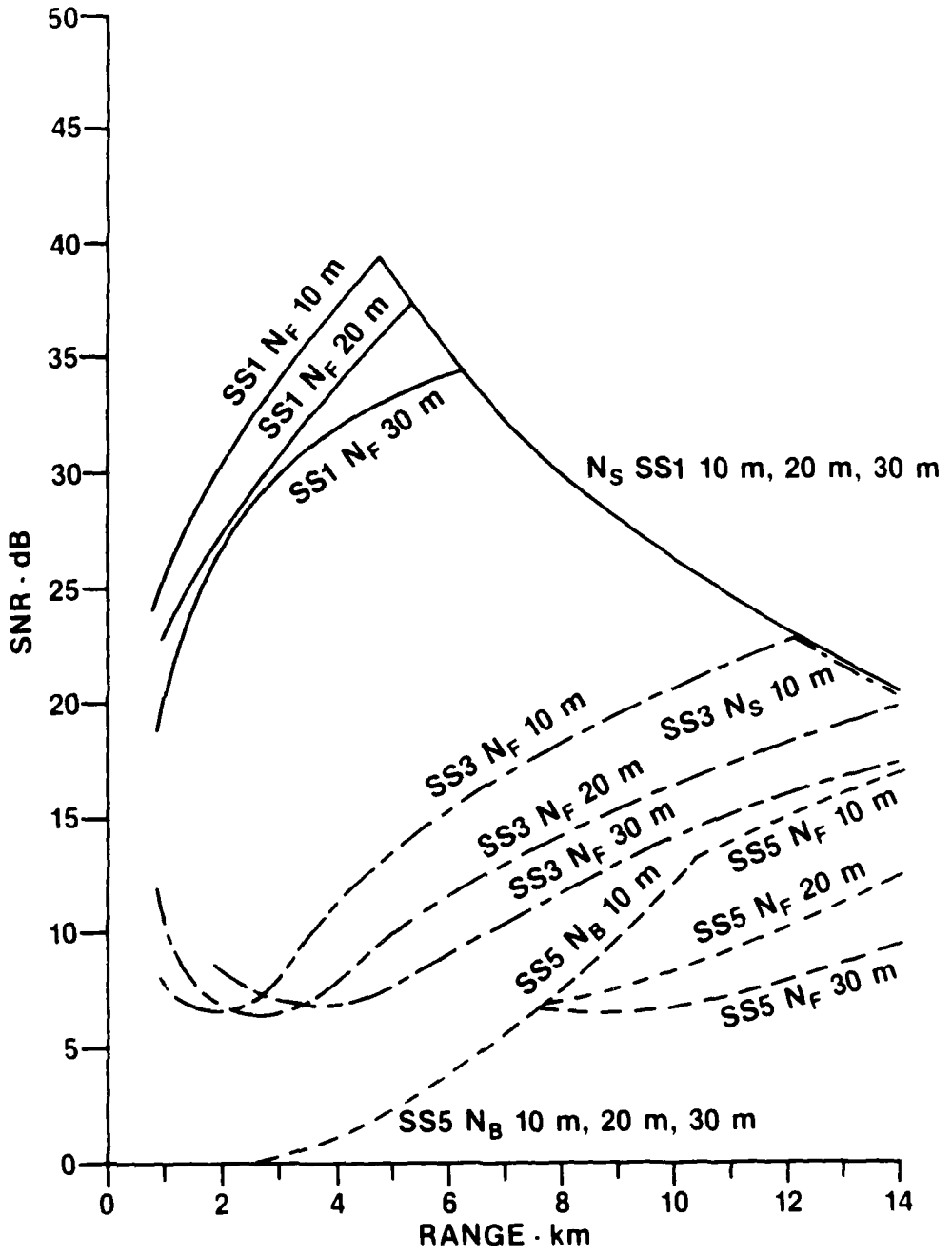

Figure 18 - Limiting SNR for Representative Sea State and Target Heights; z_1 = 10 m.

analogous to temporal frequency. Expressions have been developed and presented describing SAMPAR signals for a conventional configuration using COHOs and STALOs to maintain phase coherence and an experimental system employing a self-cohering scheme. In both cases the radar signals are shown to contain an interference term, when the radar is used in a multipath environment, in which all of the information used during CHA processing is contained. Pre-processing of the interference term is required to optimize the CHA analysis. The pre-processing involves data correction for phase and amplitude errors, data reduction (SNR enhancement) and signal normalization. Doppler pre-processing is required with CHA processing in practice in order to achieve good performance.

A discussion is given of the coherence requirement for MTI and Doppler processing in CHA-SAMPAR system. A fairly extensive discussion of SNR has been presented for a typical SAMPAR system tracking a target with a cross section of 1 m^2. In this discussion target geometries typical of sea skimmers were considered, in addition to probable sea-state conditions. Furthermore, three sources of noise have been considered, i.e. (a) system noise, (b) back-scatter clutter, and (c) forward scatter clutter. It has been shown that back-scatter clutter is the dominant noise source for high sea-states and ranges less than about 6 km. Forward-scatter clutter is the dominant noise source for most target sea-state scenarios except for low sea-state conditions, where system noise becomes dominant.

6. REFERENCES

[1] Ruvin, A.E. and L. Weinburg, "Digital multiple beamforming techniques for radar", IEEE Conf. Publ. EASCON 78, pp. 152-163, 1978.

[2] Skolnik, M.I.' "Introduction to radar systems", 2nd Ed. p. 105, McGraw-Hill Book Co., 1980.

[3] Griffiths, J.W.R., "Adaptive array processing - a tutorial", IEE Proc., Vol. 130, Pts. F andH, No. 1, February 1983.

[4] Rook, B.J. and J. Litva, "An Improved CHA Algorithm for Tracking Low-Angle Targets", CRC Report No. 1356, April 1982.

[5] I.N. El-Behery and R.H. MacPhie, "Maximum Likelihood Estimation of the Number, Directions and Strengths of Point Radio Sources from Variable Baseline Interferometer Data", IEEE Trans. On Antenna and Prop., Vol. AP-26, No. 2, March 1978, pp. 294-301.

[6] Jenkins, F.W. and H.E. White, "Fundamentals of Optics", McGraw-Hill Book Co., New York, New York, 1957.

[7] Hayden, E.C., "Propagation studies using direction-finding techniques", J. Res. NBS, Vol. 65D, No. 3, May-June 1961.

[8] Fines, N.R., "Application of Digital Beamforming with a Height Gain Pofiler", CRC Report to be published.

[9] Harris, M.A., "Fire-control radars gets rain insurance", Electronics, pp. 52-54, January 26, 1984.

[10] Skolnik, M.I., Editor, "Radar Handbook", McGraw-Hill Book Company, New York, New York, 1970.

[11] Bales, S.L., W.T. Lee and J.A. Voelker, "Standardized wave and wind environments for NATO operational areas", D.W. Taylor Naval Ship R&D Center Report No. DTNSRDC/SPD-0919-01, Unclassified, July 1981.

[12] Barton, D.K., "Radars vol. 5 - radar clutter", Ed. D.K. Barton, Artech House Inc, p. 58, 1975.

[13] Barton, D.K., "Radar system analysis", Prentice-Hall, Inc., p. 96 (equ. 3.21), April 1965.

[14] Beckmann, P. and A. Spizzichino, "The scattering of EM waves from rough surfaces", New York: Pergamon, 1963.

[15] Beard, C.I., "Coherent and incoherent scattering of microwaves from the ocean", IRE Trans. Antenna Propagat., vol. AP-9, pp. 470-483, Sept. 1961.

[16] Fishback, W.T., "Methods for calculating field strength with standard refraction", MIT Radiation Laboratory Series, Vol. 13 (Ed. D.E. Kerr), pp. 112-117, 1951.

[17] Abraham, D., "Numerically modelling sea back-scatter coefficients", Microwaves & RF, pp. 73, April 1983.

7. ACKNOWLEDGEMENT

The authors wish to thank Mr. Gordon Marwood and Dr. Ross Turner for reviewing this report and for providing helpful comments. This work was supported by the Department of National Defence, Ottawa, Canada, under Research and Development Project 011LA.

DOCUMENT CONTROL DATA

(Security classification of title, body of abstract and indexing annotation must be entered when the overall document is classified)

1. ORIGINATOR (the name and address of the organization preparing the document. Organizations for whom the document was prepared, e.g. Establishment sponsoring a contractor's report, or tasking agency, are entered in section 8.)

Communications Research Centre, Radar Research
P.O. Box 11490, Station H
Ottawa, Ontario, K2H 8S2

2. SECURITY CLASSIFICATION (overall security classification of the document, including special warning terms if applicable)

UNCLASSIFIED

3. TITLE (the complete document title as indicated on the title page. Its classification should be indicated by the appropriate abbreviation (S,C,R or U) in parentheses after the title.)

Phase Coherence and Signal-to-Noise Ratio Considerations for Sampled Aperture Radar Systems

4. AUTHORS (Last name, first name, middle initial. If military, show rank, e.g. Doe, Maj. John E.)

LITVA, J. and CHAN, H.C.

5. DATE OF PUBLICATION (month and year of publication of document)

January 1988

6a. NO. OF PAGES (total containing information. Include Annexes, Appendices, etc.)

42

6b. NO. OF REFS (total cited in document)

17

7. DESCRIPTIVE NOTES (the category of the document, e.g. technical report, technical note or memorandum. If appropriate, enter the type of report, e.g. interim, progress, summary, annual or final. Give the inclusive dates when a specific reporting period is covered.)

CRC Report No. 1412

8. SPONSORING ACTIVITY (the name of the department project office or laboratory sponsoring the research and development. Include the address.)

Defence Research Establishment Ottawa
Ottawa, Ontario, K1A 0Z4

9a. PROJECT OR GRANT NO. (if appropriate, the applicable research and development project or grant number under which the document was written. Please specify whether project or grant)

011LA

9b. CONTRACT NO. (if appropriate, the applicable number under which the document was written)

10a. ORIGINATOR'S DOCUMENT NUMBER (the official document number by which the document is identified by the originating activity. This number must be unique to this document.)

10b. OTHER DOCUMENT NOS. (Any other numbers which may be assigned this document either by the originator or by the sponsor)

11. DOCUMENT AVAILABILITY (any limitations on further dissemination of the document, other than those imposed by security classification)

(xx) Unlimited distribution
( ) Distribution limited to defence departments and defence contractors; further distribution only as approved
( ) Distribution limited to defence departments and Canadian defence contractors; further distribution only as approved
( ) Distribution limited to government departments and agencies; further distribution only as approved
( ) Distribution limited to defence departments; further distribution only as approved
( ) Other (please specify):

12. DOCUMENT ANNOUNCEMENT (any limitation to the bibliographic announcement of this document. This will normally correspond to the Document Availability (11). However, where further distribution (beyond the audience specified in 11) is possible, a wider announcement audience may be selected.)

13. ABSTRACT (a brief and factual summary of the document. It may also appear elsewhere in the body of the document itself. It is highly desirable that the abstract of classified documents be unclassified. Each paragraph of the abstract shall begin with an indication of the security classification of the information in the paragraph (unless the document itself is unclassified) represented as (S), (C), (R), or (U). It is not necessary to include here abstracts in both official languages unless the text is bilingual).

This report describes the application of Sampled Aperture Radar (SAMPAR) technology to the tracking of low-angle targets at sea. In particular, expressions are developed and presented describing aperture signals for a conventional (SAMPAR) configuration which uses coherent local oscillators. The radar signals are shown to contain an interference term in which is contained all of the information used during Correlation Height Analysis (CHA) processing. A continuous wave (CW) experiment designed to evaluate the CHA algorithm is described. This system employs a beacon source and self-cohering receivers. It is shown that the same interference term is also contained in the self-cohered received signal. Some pre-processing of the interference term is required prior to CHA processing to optimize the results. A discussion is given of the implementation of Doppler processing for various target velocities. Finally a discussion is given of signal-to-noise ratios for typical target geometries and sea-state conditions, in which forward-scatter clutter, back-scatter clutter and system noise are taken into account.

14. KEYWORDS, DESCRIPTORS or IDENTIFIERS (technically meaningful terms or short phrases that characterize a document and could be helpful in cataloguing the document. They should be selected so that no security classification is required. Identifiers, such as equipment model designation, trade name, military project code name, geographic location may also be included. If possible, keywords should be selected from a published thesaurus, e.g. Thesaurus of Engineering and Scientific Terms (TEST) and that thesaurus identified. If it is not possible to select indexing terms which are Unclassified, the classification of each should be indicated as with the title.)

Coherence

Sampled-Aperture

Radar